

## Nonlinear Controls on the Persistence of La Niña\*

PEDRO N. DINEZIO

*International Pacific Research Center, School of Ocean and Earth Science and Technology,  
University of Hawai'i at Mānoa, Honolulu, Hawaii*

CLARA DESER

*National Center for Atmospheric Research,<sup>†</sup> Boulder, Colorado*

(Manuscript received 31 December 2013, in final form 30 June 2014)

### ABSTRACT

A large fraction (35%–50%) of observed La Niña events last two years or longer, in contrast to the great majority of El Niño events, which last one year. Here, the authors explore the nonlinear processes responsible for the multiyear persistence of La Niña in the Community Climate System Model, version 4 (CCSM4), a coupled climate model that simulates the asymmetric duration of La Niña and El Niño events realistically. The authors develop a nonlinear delayed-oscillator (NDO) model of the El Niño–Southern Oscillation (ENSO) to explore the mechanisms governing the duration of La Niña. The NDO includes nonlinear and seasonally dependent feedbacks derived from the CCSM4 heat budget, which allow it to simulate key ENSO features in quantitative agreement with CCSM4.

Sensitivity experiments with the NDO show that the nonlinearity in the delayed thermocline feedback is the sole process controlling the duration of La Niña events. The authors' results show that, as La Niña events become stronger, the delayed thermocline response does not increase proportionally. This nonlinearity arises from two processes: 1) the response of winds to sea surface temperature anomalies and 2) the ability of thermocline depth anomalies to influence temperatures at the base of the mixed layer. Thus, strong La Niña events require that the thermocline remains deeper for longer than 1 yr for sea surface temperatures to return to neutral. Ocean reanalysis data show evidence for this thermocline nonlinearity, suggesting that this process could be at work in nature.

### 1. Introduction

A large fraction (35%–50%) of La Niña events last two years or longer (Okumura and Deser 2010) in contrast to El Niño events, which rarely last longer than one year. The multiyear persistence of La Niña exacerbates its global climate impacts, especially in regions prone to

drought. Several observational studies have documented the asymmetry in the duration of the two phases of El Niño–Southern Oscillation (ENSO) (e.g., Kessler 2002; Larkin and Harrison 2002; McPhaden and Zhang 2009; Ohba and Ueda 2009; Wu et al. 2010; Okumura and Deser 2010; Ohba et al. 2010; Hu et al. 2013). For instance, during the 1980–2008 period, sea surface temperature (SST) observations show that La Niña tends to persist into a second year, reintensifying during the following boreal winter (McPhaden and Zhang 2009). Observations also show that warm-to-cold transitions tend to occur within a single year, in contrast to the cold-to-warm transitions, which occur over 1–3 yr (Larkin and Harrison 2002; Kessler 2002).

Simple conceptual models of ENSO, such as the delayed oscillator (Suarez and Schopf 1988, hereafter SS88; Battisti and Hirst 1989, hereafter BH89) or the recharge oscillator Jin (1997, hereafter J97), posit that the delayed thermocline response to anomalies of one

---

\* School of Ocean and Earth Science and Technology Publication Number 9166 and International Pacific Research Center Publication Number 1068.

<sup>†</sup> The National Center for Atmospheric Research is sponsored by the National Science Foundation.

---

*Corresponding author address:* Pedro N. DiNezio, International Pacific Research Center, School of Ocean and Earth Science and Technology, University of Hawai'i at Mānoa, 1680 East-West Rd., Honolulu, HI 96822.  
E-mail: pdn@hawaii.edu

sign drive the transition into SST anomalies of the opposite sign. However, some of the observational studies mentioned above suggest that this relationship between thermocline and SST anomalies breaks down during La Niña (Kessler 2002; Nagura et al. 2008; McPhaden and Zhang 2009). Observations show that, for 40% of its cycle, ENSO is characterized by negative SST anomalies (i.e., La Niña), along with deeper thermocline anomalies (Kessler 2002). This suggests an asymmetry in ENSO dynamics since this phase should take 25% of the ENSO cycle if the dynamics were linear/symmetric.

The physical processes causing the asymmetric duration of ENSO events are unclear. Ohba and Ueda (2009) and Okumura et al. (2011) argue that it is caused by wind anomalies that are shifted westward and of weaker magnitude during La Niña events. This asymmetric wind response occurs because of differences in the location of precipitation anomalies over the western Pacific between El Niño and La Niña, resulting in wind anomalies of different magnitudes (Ohba and Ueda 2009; Frauen and Dommenget 2010; Okumura et al. 2011). Choi et al. (2013) also showed that this nonlinearity plays a role in the asymmetric duration of ENSO events, however, by influencing the termination of La Niña through the delayed adjustment of the thermocline to wind anomalies. Hu et al. (2013) argue that ocean dynamical processes involving Kelvin and Rossby waves are key for the persistence of La Niña, but the causes for the persistence of wind anomalies over the western Pacific remain unclear from their study.

These studies have focused on atmospheric or ocean processes separately, but the asymmetric duration of ENSO events has not been examined in a coupled framework. Furthermore, investigation of this feature using general circulation coupled models is hindered by the fact that few models can simulate the persistence of La Niña realistically (Ohba et al. 2010). Among them, the Community Climate System Model, version 4 (CCSM4), simulates many features of La Niña observed in nature (Deser et al. 2012). Long-lived La Niña events simulated by CCSM4 show negative SST anomalies persisting in the central equatorial Pacific during boreal spring, re-intensifying during winter of the second year (Fig. 1). CCSM4 also simulates the frequency of occurrence of these events realistically since one out of three simulated events persists for 2 yr or longer as observed in the historical record (Deser et al. 2012).

CCSM4 simulates ENSO events with many characteristics of an oscillation between SST anomalies and thermocline depth anomalies, as conceptualized in the SS88 and BH89 delayed oscillator (DO) or in J97's recharge oscillator (RO). ENSO events with La Niña conditions lasting for 1 yr (1-yr LN) exhibit zonally averaged

thermocline depth anomalies  $\bar{Z}_{tc}$ , leading SST anomalies during the transition from El Niño to La Niña and during the transition from La Niña to neutral conditions, consistent with linear ENSO dynamics (Fig. 2a). ENSO events with La Niña conditions lasting at least 2 yr (2-yr LN) also exhibit  $\bar{Z}_{tc}$  anomalies preceding SST anomalies during the transition from El Niño to La Niña; however, this lead-lag relationship breaks down after the first peak of La Niña. During this phase of the ENSO cycle, the thermocline deepens and cold SST anomalies persist, very much as observed (Kessler 2002). La Niña conditions peak again in the following year (Fig. 2b) and return to neutral conditions after a total of 2 yr with an anomalously deeper thermocline.

This preliminary analysis suggests that the thermocline is involved in the multiyear persistence of La Niña. Throughout the rest of the study, we systematically explore the nonlinear processes controlling the duration of La Niña using output from the 1300-yr control simulation performed with CCSM4. We first perform a heat budget analysis of ENSO as simulated by CCSM4. We use the heat budget results to develop a nonlinear version of the delayed-oscillator model of Battisti and Hirst (1989), in which the Bjerknes and delayed thermocline feedbacks, as well as the atmospheric damping, are nonlinear functions of Niño-3.4 SST anomalies. We then perform a series of experiments with the nonlinear delayed-oscillator (NDO) model in order to isolate the effects of the nonlinear feedbacks on the duration of La Niña and thus diagnose the physical processes responsible for its multiyear persistence. The NDO experiments show that a nonlinearity in the delayed thermocline feedback is the sole process controlling the duration of La Niña in the NDO. We conclude with a discussion of the processes giving rise to this nonlinearity in CCSM4 and in ocean reanalysis, along with precursors that could be used to anticipate whether La Niña will persist into a second year.

## 2. Data

### a. CCSM4 long control simulation

The data used in our analysis are from a 1300-yr control simulation of preindustrial climate performed with the CCSM4. CCSM4 is a climate model consisting of coupled atmosphere and ocean general circulation models (GCMs) and comprehensive land and cryosphere models. The reader is referred to Gent et al. (2011) for specific information about CCSM4. The control simulation analyzed here includes interactions between components of the climate system (ocean, atmosphere, cryosphere, and land) configured at nominal 1° latitude–longitude resolution

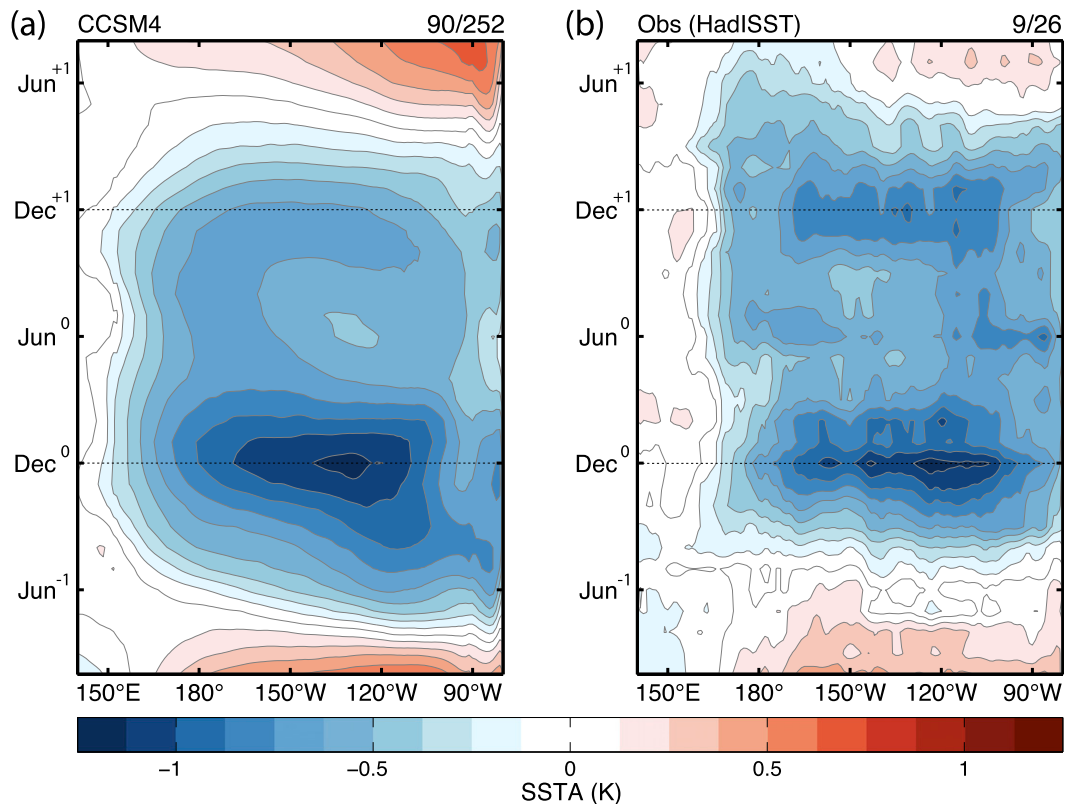


FIG. 1. Longitude–time evolution of (a) simulated and (b) observed sea surface temperature anomalies (SSTA) for 2-yr La Niña events. Simulated SSTA are from the CCSM4 1300-yr-long control simulation. Observed SSTA are from HadISST (Rayner et al. 2003) for the 1880–2010 period. SSTA are averaged over the 5°S–5°N equatorial band for observations. The 2-yr La Niña events are selected and composited following the methodology described in section 2d for both observations and CCSM4. The number at the top of each panel indicates the number of 2-yr events out of the total number of La Niña events. The model composite is scaled by a factor of 1.3 to match the observed composite amplitude of the Niño-3.4 SST index in December of year 0.

and forced by constant preindustrial greenhouse gas concentrations. The simulated ENSO exhibits several features observed in nature, such a 3–6-yr period, decadal variations in amplitude and frequency, stronger El Niño compared with La Niña, and longer duration of La Niña compared to El Niño (Deser et al. 2012). Although El Niño events appear to have different initiation mechanisms in CCSM4 and observations (Deser et al. 2012), La Niña events are driven by thermocline depth anomalies in both CCSM4 and nature. Therefore, we consider the CCSM4 simulation sufficiently realistic to study the dynamics of the multiyear persistence of La Niña.

#### b. Observational datasets

The following observational datasets are used: 1) SST from the Hadley Centre Sea Ice and SST dataset, version 1.1 (HadISST1.1), (Rayner et al. 2003) during 1880–2013 on a  $1^\circ \times 1^\circ$  longitude–latitude grid and 2) upper-ocean temperature and surface wind stress from the European Centre for Medium-Range Weather Forecasts (ECMWF)

Ocean Reanalysis System 4 (ORAS4) for the period 1960–2011 (Balmaseda et al. 2013). ORAS4 assimilates temperature and salinity profiles and along-track altimeter-derived sea level anomalies on a  $1^\circ \times 1^\circ$  longitude–latitude grid with progressively finer latitude resolution ( $0.3^\circ$ ) in the tropics and 42 levels in the vertical (18 of which are in the upper 200 m). The ORAS4 is driven by winds from the 40-yr ECMWF Re-Analysis (ERA-40) until 1989, the Interim ECMWF Re-Analysis (ERA-Interim) from 1989 to 2010, and the ECMWF NWP analysis thereafter. ORAS4 also uses observed SST, sea surface salinity, sea ice, and global-mean sea level to correct biases in the heat and freshwater budgets.

#### c. Niño-3.4 SST index

The Niño-3.4 SST index is computed by averaging SST anomalies over the Niño-3.4 region located in the central Pacific (5°S–5°N, 120°–170°W). All anomalies are computed with respect to the monthly-mean seasonal cycle. The Niño-3.4 region is ideally located to capture SST

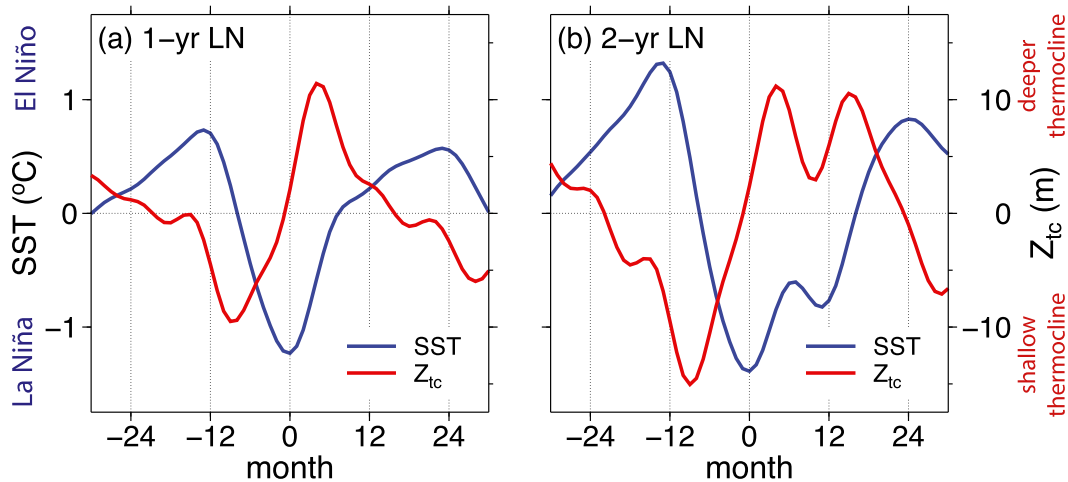


FIG. 2. Composite sea surface temperature (blue) and zonal-mean thermocline depth (red) anomalies for (a) 1-yr and (b) 2-yr La Niña events simulated by CCSM4. Month 0 coincides with the first-year peak of La Niña. The sea surface temperature anomalies are averaged over the Niño-3.4 region ( $5^{\circ}\text{S}$ – $5^{\circ}\text{N}$ ,  $120^{\circ}$ – $170^{\circ}\text{W}$ ). The thermocline depth anomalies are zonally averaged across the equatorial Pacific ( $5^{\circ}\text{S}$ – $5^{\circ}\text{N}$ ,  $140^{\circ}\text{E}$ – $80^{\circ}\text{W}$ ). Positive anomalies indicate a deeper thermocline and negative anomalies indicated a shallower thermocline. Further details on the methodology to compute anomalies and select 1- and 2-yr La Niña events may be found in section 2.

variations associated with La Niña events because their amplitude is largest there. In addition, owing to the presence of strong east–west gradients in both climatological SST and thermocline depth, the central Pacific is where coupling between SST, wind, and thermocline anomalies—the Bjerknes feedback—is most effective (Schopf and Suarez 1988). Interannual anomalies are isolated after removing the climatological seasonal cycle and smoothing using a fifth-order bandpass Butterworth filter with cutoff frequencies of 2 and  $0.1 \text{ yr}^{-1}$  (6-month to 10-yr periods).

#### d. Two-year La Niña events

We identify La Niña events by selecting local minima of the Niño-3.4 SST index exceeding 0.75 standard deviations in magnitude. The standard deviation of the Niño-3.4 index in the 1300-yr CCSM4 control simulation is 0.99 K. Before selecting the events, we smooth the Niño-3.4 index using a fifth-order bandpass Butterworth filter with cutoff frequencies of 1 and  $0.1 \text{ yr}^{-1}$ . This filter isolates interannual signals by removing subseasonal and decadal variability to unambiguously detect the minima associated with La Niña events. Only local minima occurring from October to February are considered. To identify the first year of all La Niña events, we apply an additional criterion that the value of the Niño-3.4 SST index is greater than  $-0.5$  standard deviations 12 months before (e.g., not La Niña). A total of 252 La Niña events are identified in the 1300 years of model data after applying these conditions. Then we select La Niña events lasting 2 yr or more (2-yr LN events) as those exhibiting La Niña conditions persisting into boreal

winter of the following year. We identify these events by requiring that the Niño-3.4 SST index be less than  $-0.5$  standard deviation 12 months after the first-year peak of La Niña. A total of 90 events (35% of the La Niña events) satisfy this condition. We also identify 1-yr LN events by requiring that the Niño-3.4 SST index be greater than  $-0.5$  standard deviations 12 months after the first-year peak of La Niña.

Persistent La Niña events in the model occur in the same proportion as those in nature based on the HadISST data for the 1880–2013 period, during which 9 out of 26 La Niña events (35%) persisted for 2 yr or longer. Note that 50% of observed La Niña events lasted 2 yr or longer during the 1950–2010 period (Okumura and Deser 2010). This value is not inconsistent with the CCSM4 simulation because the frequency of occurrence of *simulated* 2-yr LN exhibits remarkable century-to-century variations. According to the CCSM4 long control run, intervals of 100 yr exhibiting 50% of 2-yr LN events are not uncommon (Fig. 3), with century-to-century variations ranging from 10% to 70%.

#### e. Zonal-mean thermocline depth

In the tropical Pacific, the depth of the  $20^{\circ}\text{C}$  isotherm (D20) is often used to study interannual changes in the depth of the thermocline  $Z_{\text{tc}}$ . However, D20 is not a material surface and can be influenced by diabatic processes such as surface heating. This could become a problem in the equatorial cold tongue where the thermocline is very close to the surface and may be influenced by air–sea buoyancy fluxes. Using the depth of an isotherm could also

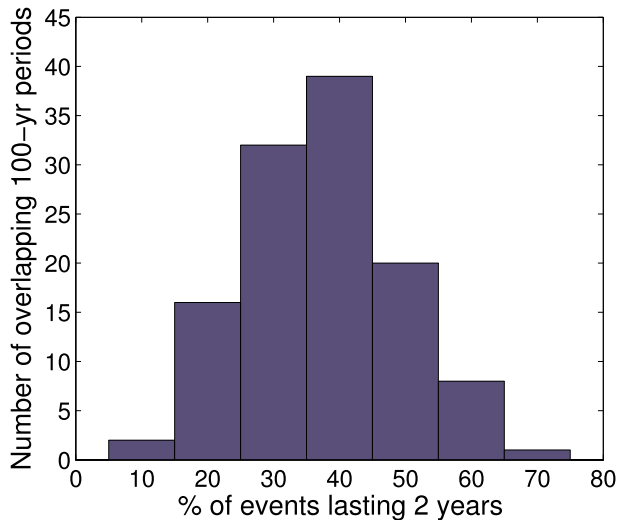


FIG. 3. Histogram of the percentage of La Niña events lasting two years in overlapping 100-yr periods from the CCSM4 1300-yr control simulation.

be problematic in climate models because the 20°C isotherm may not necessary lie within the model's

thermocline owing to model biases. For these reasons, we define  $Z_{\text{tctc}}$  as the depth of the maximum vertical temperature gradient. We define a zonal-mean thermocline index ( $\bar{Z}'_{\text{tc}}$ ) by averaging  $Z'_{\text{tc}}$  over the equatorial Pacific defined as 5°S–5°N, 140°–80°W. Interannual anomalies are isolated after removing the climatological seasonal cycle and smoothing using a fifth-order bandpass Butterworth filter with cutoff frequencies of 2 and 0.1 yr<sup>-1</sup> (6-month to 10-yr periods).

#### f. Heat budget

We perform a heat budget analysis in order to diagnose the physical processes involved in the persistence and termination of La Niña. The methodology used to estimate the different terms of the temperature equation has been used to study ENSO dynamics in coupled GCMs (DiNezio et al. 2009, 2012; Capotondi 2013). The most important feature of this methodology is that a nearly balanced heat budget can be obtained using monthly-mean three-dimensional velocity ( $u, v, w$ ) and temperature ( $T$ ) fields. Our analysis of the full heat budget shows that for interannual anomalies the heat budget can be approximated by

$$\rho_0 c_p H \frac{\partial [T']}{\partial t} \cong -\rho_0 c_p \int_{-H}^0 \left( u' \frac{\partial \bar{T}}{\partial x} + w' \frac{\partial \bar{T}}{\partial z} + \bar{w} \frac{\partial T'}{\partial z} + u' \frac{\partial T'}{\partial x} \right) dz + Q'_{\text{atm}}. \quad (1)$$

The definitions of the variables in (1) follow the convention where primed variables are anomalies with respect to the climatological monthly-mean seasonal cycle (overbar variables). We neglect several temperature advection terms, such as meridional advection and most nonlinear terms, because their interannual variability is small. Both tendency and advection terms are integrated over a constant-depth layer of thickness  $H$ , which is taken to be 20 m below the base of the ocean mixed layer (similar results are obtained using 10–30 m). For the Niño-3.4 region, the base of the mixed layer is approximately 80 m; thus, we select  $H = 100$  m. The term  $[T']$  is the ocean temperature anomaly averaged over depth  $H$ . Selecting  $H$  below the base of the mixed layer allows us to neglect the effect of subgrid-scale (SGS) processes, such as wind-driven mixing and entrainment and sunlight penetration on  $[T']$ . Our rationale for this approximation is as follows: These are first-order processes within the ocean mixed layer, but their importance decreases with depth. The effect of these processes on  $T'$  is represented as the convergence of a heat flux ( $F'_{\text{sgs}}$  and  $F'_{\text{sw}}$ ), and therefore their vertical integral in (1) reduces to the value of  $F'_{\text{sgs}}$  and  $F'_{\text{sw}}$  at  $z = H$  multiplied by the layer thickness  $H$ . The  $F'_{\text{sgs}}$  and  $F'_{\text{sw}}$  are negligible at  $z = H$  [not shown here, but see Fig. A1 in DiNezio et al. (2009)] and

thus we neglect their associated heat flux convergence in (1). At the same time, averaged over the Niño-3.4 region,  $[T']$  approximates the Niño-3.4 SST index very well (correlation = 0.98; slope = 0.96). The heat budget in (1) is completed with  $Q'_{\text{atm}}$ , the net air–sea heat flux (positive into the ocean). The remaining constants are  $\rho_0$ , a reference density of seawater, and  $c_p$ , the specific heat of seawater.

Throughout this study, we focus on the heat budget terms averaged over the Niño-3.4 region because this is where the Bjerknes feedback is strongest and therefore where nonlinearities in the ENSO feedbacks will influence the dynamics of La Niña. The Niño-3.4 time series of each term of (1) are smoothed using a bandpass filter with cutoff frequencies between 2 and 0.1 yr<sup>-1</sup> (6-month to 10-yr periods) in order to isolate the effect of these tendencies on interannual SST variability. Averaged over Niño-3.4 region, the left-hand side (lhs) and right-hand side (rhs) of (1) exhibit a correlation of  $r = 0.93$  over the full 1300-yr CCSM4 dataset. Therefore, (1) is a very accurate approximation of the full SST equation.

### 3. Nonlinearities in the ENSO heat budget

In this section, we show that the advection terms of (1) are related to ENSO feedbacks in the following way.

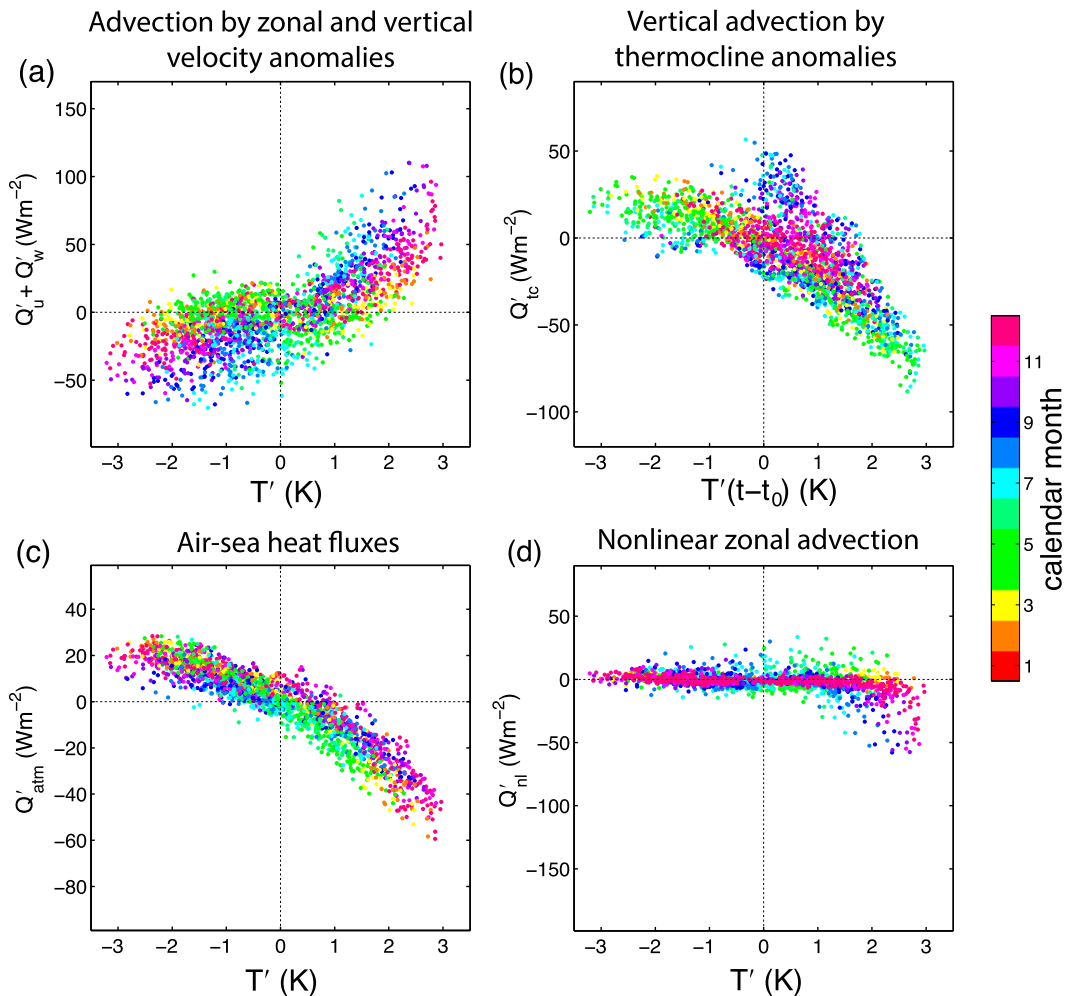


FIG. 4. Nonlinearities in the terms of the heat budget. Scatterplots between SST anomalies averaged over the Niño-3.4 region ( $x$  axis) and (a) the advection of the climatological temperature gradients by zonal and vertical velocity anomalies ( $Q'_u + Q'_w$ ), (b) the advection of the vertical temperature gradient anomalies by the climatological upwelling ( $Q'_{tc}$ ), (c) air-sea fluxes ( $Q'_{atm}$ ), and (d) nonlinear zonal advection ( $Q'_{nl}$ ) ( $y$  axis). The  $Q'_{tc}$  is plotted against the lagged SST anomalies [ $T'(t - t_0)$ ] since it leads SST anomalies by about  $t_0 = 6$  months. Colors indicate calendar months in order to highlight the seasonal modulation of the nonlinearities of the heat budget terms. Further details on the methodology to compute the anomalies may be found in [section 2f](#).

- (i) The advection of the climatological temperature gradient by vertical velocity anomalies ( $Q'_w = -\rho_0 c_p \int_{-H}^0 w' \partial \bar{T} / \partial z dz$ ) and part of the temperature advection by zonal current anomalies ( $Q'_u = -\rho_0 c_p \int_{-H}^0 u' \partial \bar{T} / \partial x dz$ ) represent a *positive* feedback because they are positively correlated with Niño-3.4 SST anomalies (denoted as  $T'$  for consistency with the figures).
- (ii) The advection of the temperature anomalies by climatological upwelling ( $Q'_{tc} = -\rho_0 c_p \int_{-H}^0 \bar{w} \partial T' / \partial z dz$ ) and part of the temperature advection by zonal current anomalies ( $Q'_u$ ) represent a delayed *negative* feedback because they are in quadrature with  $T'$  (i.e., positively correlated with  $Z_{tc}$  anomalies).

Further details on the evolution of  $Q'_u$  and  $Q'_{tc}$  during the simulated La Niña are provided in [appendix A](#).

- (iii) Net air-sea heat flux ( $Q'_{atm}$ ) is anticorrelated with  $T'$  and therefore represents a *negative* feedback.
- (iv) Nonlinear zonal advection ( $Q'_{nl} = -\rho_0 c_p \int_{-H}^0 u' \partial T' / \partial x dz$ ) is anticorrelated with  $T'$  but only for El Niño events, and it therefore represents a *negative* feedback.

These correlations are clearly seen in scatterplots of the different terms of the heat budget (1) versus the Niño-3.4 SST anomalies (Fig. 4). The  $Q'_u$  and  $Q'_w$  are positively correlated with Niño-3.4 SST anomalies, but

in a markedly nonlinear way. The  $Q'_u + Q'_w$  anomalies are much larger for El Niño ( $T' > 0$ ) than for La Niña ( $T' < 0$ ) (Fig. 4a). This nonlinearity appears to be related to the response of zonal winds (the driver of  $u'$  and  $w'$ ), which is stronger for positive  $T'$  than for negative  $T'$  (not shown). This wind–SST nonlinearity has been linked to the effect of background SST on the convective response, which leads to a much larger convective response for warm anomalies (Hoerling et al. 1997; Kang and Kug 2002; Frauen and Dommenges 2010). The strength of the associated positive feedback (given by the slope of the scatterplot) appears to be modulated by the seasonal cycle, with the largest values in boreal summer (June–August) (Fig. 4a: light blue and blue dots).

The advection of vertical temperature anomalies by the climatological upwelling  $Q'_{tc}$  is anticorrelated with  $T'$  at a lag  $t_0$  of 6 months (computed by optimizing the lagged correlation between  $Z'_{tc}$  and  $T'$ ). The scatterplot (Fig. 4b) shows that  $Q'_{tc}$  becomes negative 6 months after El Niño [ $T'(t - t_0) > 0$ ] and, conversely,  $Q'_{tc}$  becomes positive 6 months after La Niña [ $T'(t - t_0) < 0$ ]. This delayed response drives a negative  $T'$  tendency that acts as a negative feedback. The dependence of  $Q'_{tc}$  on  $T'(t - t_0)$  is also markedly nonlinear, with a much larger magnitude of  $Q'_{tc}$  in response to El Niño [ $T'(t - t_0) > 0$ ] than to La Niña [ $T'(t - t_0) < 0$ ]. The relationship between  $Q'_{tc}$  on  $T'(t - t_0)$  also exhibits seasonal dependence: it is largest during boreal spring (April–June: green dots), when the climatological upwelling  $\bar{w}$  is strongest, and smallest during boreal fall and winter (September–January, purple and red dots) when  $\bar{w}$  is weakest (not shown).

Thermocline anomalies play a role in both the positive Bjerknes feedback and the negative delayed thermocline feedback. The effect of the thermocline on these feedbacks is spatially dependent. Thermocline anomalies contribute to the Bjerknes feedback in the eastern Pacific where it deepens (shoals) during El Niño (La Niña) as the east–west tilt of the thermocline relaxes (strengthens) in response to weaker (stronger) trade winds. This response, however, is negligible in the central Pacific (i.e., the Niño-3.4 region) because this region straddles the centers of action of the thermocline tilt. In contrast, the delayed negative effect has an effect on the central Pacific because it is associated with thermocline anomalies that are zonally uniform. This explains why  $Q'_{tc}$  averaged over the Niño-3.4 region is anticorrelated with  $T'(t - t_0)$ , consistent with the *negative* delayed thermocline feedback, but exhibits a low correlation with  $T'$  as expected from the *positive* Bjerknes feedback.

Note that the scatter in Fig. 4b is mostly due to seasonal modulation of  $Q'_{tc}$  by  $\bar{w}$ . When the results are stratified by

calendar month, the anticorrelation between  $Q'_{tc}$  and  $T'(t - t_0)$  is more evident ( $r < -0.9$ ), with pronounced nonlinearity from January to June (Fig. B2). For instance, during March the  $Q'_{tc}$  associated with  $T' = 2$  K is about  $-50 \text{ W m}^{-2}$ , while for  $T' = -2$  K  $Q'_{tc}$  is only about  $30 \text{ W m}^{-2}$  (Fig. B2). This asymmetry in the  $Q'_{tc}$  response between El Niño and La Niña results mainly from nonlinearities in two processes: 1) the wind–SST nonlinearity discussed above, since a weaker wind anomaly for a given  $T'$  would lead to a weaker delayed  $Z'_{tc}$  response, and 2) the influence of thermocline anomalies on the near-surface stratification anomalies ( $\partial T'/\partial z$ ). The effect of these nonlinearities on the delayed thermocline feedback will be discussed in section 6a.

The dependence of the air–sea heat fluxes ( $Q'_{atm}$ ) on  $T'$  is also nonlinear, with a much stronger response for El Niño ( $T' > 0$ ) than for La Niña ( $T' < 0$ ) (Fig. 4c). The  $Q'_{atm}$  is largest during boreal spring (March–May) when the climatological SST gradient is weakest and background SSTs are seasonally warmer (Fig. 4c, yellow–green dots). Conversely,  $Q'_{atm}$  is smallest during boreal fall (September–October), when the climatological SST gradient is strongest and background SSTs are seasonally colder (Fig. 4c: blue dots). Analysis of cloud properties over the Niño-3.4 region suggests that the nonlinearity of  $Q'_{atm}$  is intimately related to shifts in cloud type, from high (deep) clouds during El Niño to low clouds during La Niña (not shown). High clouds exert a negative feedback on SSTs, while low clouds exert a positive feedback: hence, the asymmetric  $Q'_{atm}$  response. This asymmetry arises because the Niño-3.4 region is located between areas of very distinct cloud types: high clouds toward the west and low clouds toward the east. Therefore, SST variations through the ENSO cycle can shift these cloud regimes eastward or westward, changing the cloud type over the Niño-3.4 region and hence the  $Q'_{atm}$  response (Bellenger et al. 2014; Dommenges et al. 2014). Last, the dependence of  $Q'_{nl}$  on  $T'$  is markedly nonlinear because this term is the product of  $u'$  and  $\partial T'/\partial x$ , which are both governed by the wind–SST nonlinearity: hence, the pronounced nonlinearity of  $Q'_{nl}$  (Fig. 4d). Because of this,  $Q'_{nl}$  acts as a very effective negative feedback affecting strong El Niño events only.

#### 4. Nonlinear delayed oscillator

##### a. Growth and damping rates

In this section, we develop a nonlinear version of the SS88 and BH89 delayed oscillator in order to study the effect of nonlinear ENSO feedbacks on the duration of La Niña. The nonlinear delayed oscillator equation is

$$\frac{\partial T'}{\partial t} = aT' - bT'(t - t_0) - cT' - dT' + N(t), \quad (2)$$

where  $T'$  represents SST anomalies averaged over the Niño-3.4 region,  $t_0$  (the lag at which the anticorrelation between  $\bar{Z}'_{tc}$  and  $T'$  is at maximum) is 6 months, and  $N(t)$  is stochastic forcing that is uncorrelated with  $T'$ . Unlike the SS88 and BH89 DO, where the  $a$ ,  $b$ ,  $c$ , and  $d$  coefficients are constants, here they are nonlinear functions of  $T'$  [or  $T'(t - t_0)$ ] and calendar month. These dependencies allow the feedbacks of (2) to capture the asymmetries and seasonal dependence seen in the different terms of the CCSM4 ENSO heat budget. A similar methodology was used by Timmermann et al. (2001) and Timmermann (2003); however, the coefficients were not based on heat budget data, nor did they include seasonality.

The function  $a$  captures the effect of processes positively correlated with  $T'$ , such as  $Q'_u$  and  $Q'_w$ ; function  $b$  captures the processes anticorrelated with  $T'(t - t_0)$ , such as  $Q'_u$  and  $Q'_{tc}$ ; and function  $c$  captures the damping effect of air–sea fluxes on  $T'$ . Note that, in the SS88 and BH89 DO, the atmospheric damping term takes the form  $-cT'^3$  (where  $c$  is a positive constant), which is nonlinear but symmetric and thus unable to capture the asymmetries in atmospheric damping seen in CCSM4 (recall Fig. 4c). We also include in (2) the term  $dT'$  to capture the effect of the nonlinear advection term  $u'\partial T'/\partial x$ , which becomes large and negative for the strongest El Niño events, effectively acting as additional negative feedback. We include noise  $N(t)$ , anticipating the possibility that external stochastic forcing is required to excite NDO variability.

We derive  $a$  and  $b$  by fitting  $Q'_u$ ,  $Q'_w$ , and  $Q'_{tc}$  to exponential functions of the form  $f_m(t) = C_1 \exp(C_2 T') + C_3 \exp[C_4 T'(t - t_0)] + C_5$ . The fitting functions are dependent on both  $T'$  and  $T'(t - t_0)$  in order to capture the mixed contributions from the Bjerknes feedback and the delayed thermocline feedback seen in the  $Q'_u$  and  $Q'_{tc}$  terms of (1). We perform these fits for each calendar month  $m$  in order to capture the seasonal dependence seen in the heat budget terms (Fig. 4). We group the terms of each function  $f_m$  that depend on  $T'$  and on  $T'(t - t_0)$  in order to obtain the function corresponding to  $aT'$  and  $-bT'(t - t_0)$ , respectively. Last, we compute the growth rates  $a$  and  $b$  dividing by  $T'$  and  $T'(t - t_0)$ . We follow a similar procedure to compute  $c$  and  $d$ , which we derive by fitting  $Q'_{atm}$  and  $Q'_{nl}$  to exponential functions of the form  $f_m(t) = C_1 \exp(C_2 T') + C_3$  given that these terms depends solely on  $T'$ . Further details on the derivation of these functions using the heat budget terms is provided in appendix B.

The resulting feedback functions are nonlinear, asymmetric, and seasonally dependent and represent growth rates in the case of  $a$  and damping rates in the cases of  $b$ ,  $c$ ,

and  $d$ . The  $a$  function—the Bjerknes feedback growth rate—exhibits a pronounced asymmetry between El Niño and La Niña, with much large growth rates for El Niño ( $T' > 0$ ), in addition to being strongly modulated by the seasonal cycle (Fig. 5a). The  $b$  function—the delayed thermocline feedback damping rate—is also asymmetric, with La Niña events exhibiting much weaker damping rates than El Niño (Fig. 5b). Atmospheric damping rates  $c$  are also asymmetric between El Niño and La Niña owing to the asymmetric response of high and low clouds discussed in section 3 (Fig. 5c). Nonlinear advection  $d$  is a negative feedback for the strongest El Niño events (Fig. 5d). Last,  $a$ ,  $b$ ,  $c$ , and  $d$  are also functions of calendar month so as to capture the seasonal dependence seen in the heat budget. However, as we will show, the seasonality of the feedbacks is not required for 2-yr La Niña events to occur. This seasonal modulation of the ENSO feedbacks allows the NDO to simulate the winter-to-winter reemergence of La Niña seen in CCSM4 and in nature.

When we combine the growth and damping rates correlated with  $T'$ , we obtain a total ENSO growth rate  $\gamma = a + c + d$ . The value of  $\gamma$  is positive during late summer, indicating favorable conditions for the development of SST anomalies, and negative during late winter/spring (Fig. 5e), thus explaining the seasonal modulation of ENSO variance. Stein et al. (2010) also found seasonal modulation in a recharge oscillator model derived from observations; however, their linear model is unstable (i.e.,  $\gamma > 0$ ) during a much shorter period from August to November, in contrast to our NDO, which is unstable from April to October. Our estimate of the nonlinear ENSO growth rate derived from CCSM4 becomes negative for  $T' > 3$  (owing to the effect of  $-d$ ), thus representing a limit on the ENSO instability. Including nonlinearities and seasonality leads to a more rich interaction of the ENSO instability with external noise. In the next subsection, we show that the NDO requires external stochastic forcing to exhibit variability. Thus, despite being unstable over a wide region of parameter space (Fig. 5e,  $\gamma > 0$ ), the NDO cannot produce a self-sustained ENSO oscillation. This could explain why our results differ from previous studies, which generally found negative growth rates (i.e., a damped ENSO), possibly because they did not consider seasonality or nonlinearity (e.g., Burgers et al. 2005; Kim and Jin 2011).

### b. Effect of external noise

The NDO is completed by determining  $N(t)$ , which we define as  $N(t) = \eta_0 \Gamma(t)$ , where  $\eta_0$  is a constant to be determined and  $\Gamma(t)$  is Gaussian white noise with zero mean and unit standard deviation. We explored the

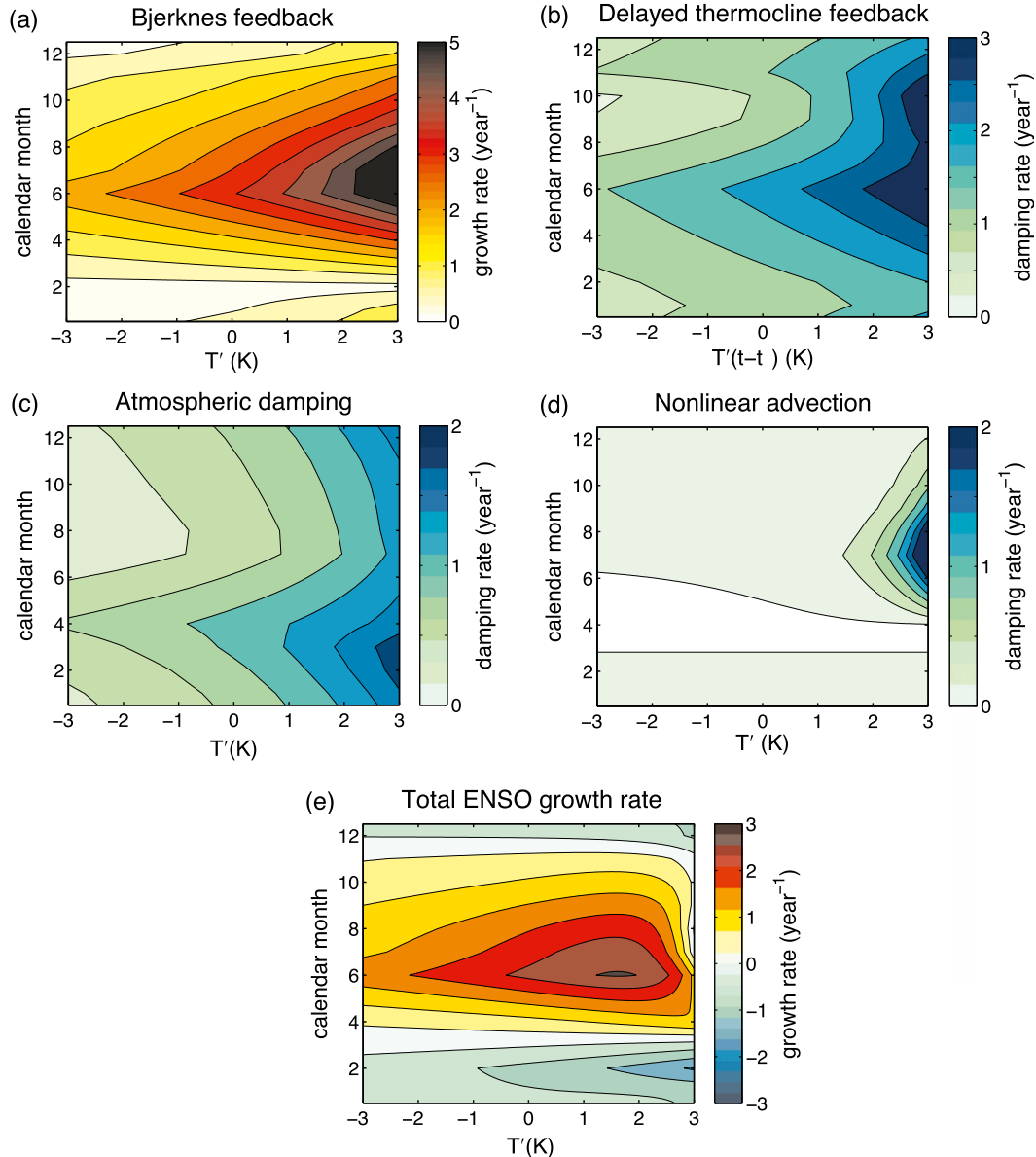


FIG. 5. Growth and damping rates ( $\text{yr}^{-1}$ ; colors) governing the nonlinear delayed-oscillator equation (2) as a function of the Niño-3.4 SST anomalies ( $x$  axis) and calendar month ( $y$  axis). (a) Growth rate  $a$  associated with the Bjerknes feedback. Damping rates (b)  $b$ , (c)  $c$ , and (d)  $d$  associated with the delayed thermocline feedback, atmospheric damping, and nonlinear advection, respectively. (e) Total growth rate  $\gamma$  resulting from the combined effect of the positive Bjerknes feedback and the negative atmospheric damping and nonlinear advection feedbacks, a measure of the NDO's instability. Positive (negative) values indicate unstable (damped) growth of Niño-3.4 SST anomalies.

sensitivity of the NDO to stochastic forcing  $N(t)$  by performing a series of simulations with  $\eta_0$  increasing from 0 to  $0.4 \text{ K month}^{-1}$ . For each value of  $\eta_0$  we compare the interannual standard deviation of the CCSM4 Niño-3.4 index with the ensemble-mean standard deviation simulated by the NDO in an ensemble of 20 realizations run for 1300 years each. Increasing the value of  $\eta_0$  leads to a monotonic increase in NDO amplitude,

measured by the interannual standard deviation. At a value of  $\eta_0 = 0.23 \text{ K month}^{-1}$ , the NDO has an interannual standard deviation of  $1.00 \pm 0.05 \text{ K}$ , which is virtually equal to that of CCSM4 ( $0.99 \text{ K}$ ).

That the variability of the NDO increases with the amplitude of the external noise suggests that the NDO resides in a stable regime; that is, external forcing is required for the NDO to exhibit variability. This is

consistent with the CCSM4 ENSO, which also appears to reside in a stable regime. The simulation of ENSO in the National Center for Atmospheric Research (NCAR) models has improved dramatically in this sense. For example, ENSO exhibited a biennial self-sustained oscillation in CCSM3, a previous version of the model. However, since version 3.5, CCSM represents ENSO as a series of events, owing to improved simulation of the meridional extent of the wind anomalies and their associated ocean response (Neale et al. 2008). In the real world, warm events also appear to arise from a stable basic state excited by stochastic forcing (Penland and Sardeshmukh 1995; Thompson and Battisti 2001; Kessler 2002). The initiating process involves subseasonal variability associated with the Madden–Julian oscillation (MJO) and westerly wind bursts (e.g., McPhaden and Yu 1999; Vecchi and Harrison 2000) but seems independent of ENSO or background state. More sophisticated representations of stochastic forcing have been proposed (e.g., Eisenman et al. 2005; Jin et al. 2007); however, our choice of white Gaussian noise with a 1-month decorrelation time scale produces an adequate simulation of the CCSM4 ENSO, given the simplicity of the model. Therefore, nonlinear and seasonally dependent feedbacks excited with Gaussian white noise appear to be the most parsimonious model of CCSM4's La Niña. For this reason, we use the  $\eta_0 = 0.23 \text{ K month}^{-1}$  version of the NDO to study the dynamics of La Niña, forgoing a systematic exploration of the full parameter space of the interaction of noise with nonlinearities.

### c. Agreement with CCSM4

After this simple fit of  $\eta_0$ , the NDO simulates several key ENSO features in quantitative agreement with CCSM4. The ENSO variance exhibits seasonal modulation as in CCSM4, with variability reaching a maximum during early boreal winter, and a minimum during early boreal summer (Fig. 6a). This feature of the NDO is strongly tied to the seasonal modulation of total ENSO growth rate  $\gamma$ , which is positive during boreal fall and negative during spring (Fig. 5e). The NDO and CCSM4 simulate El Niño events with larger amplitude than La Niña events, as shown by the positive skewness of  $0.20 \pm 0.07 \text{ K}$  and  $0.19 \text{ K}$ , respectively. The large range of skewness values simulated by each realization of the NDO suggests that, while the skewness may be determined by the asymmetry of the Bjerknes feedback, very large variations in this statistic are possible, even in 1300-yr-long simulations with constant amplitude noise and with stationary feedbacks.

The NDO simulates a spectrum of variability with a shape and amplitude in excellent agreement with

CCSM4 (Fig. 6b). The NDO simulates a broad spectral peak centered at a 3-yr period, which is shorter than the observed peak centered at 4 yr but equal to that in CCSM4. The NDO has too much power at lower frequencies, suggesting that other processes beyond tropical dynamics may be influencing tropical Pacific decadal variability in CCSM4 or that our estimates of growth and damping rates are only valid for interannual time scales and these rates may be time-scale dependent.

The NDO also simulates La Niña events lasting 2 yr in about the same proportion as in CCSM4: 35% of La Niña events are 2-yr events in CCSM4, compared to 30% in the NDO (Fig. 6c). However, the NDO simulates a larger fraction of La Niña events lasting 3 yr or longer (12%) compared to CCSM4 (2%). Finally, the temporal evolution and amplitude of 2-yr LN events simulated by the NDO are in good agreement with CCSM4, including the reemergence in the second winter (Fig. 6d).

## 5. Multiyear persistence of La Niña

All of the nonlinearities of the ENSO feedbacks encapsulated in the NDO could potentially lead to multiyear persistence of La Niña. For instance, the atmospheric damping rate  $c$  shows less effective damping of negative SST anomalies compared to positive ones [Fig. 5c,  $T'(t - t_0) < 0$ ], potentially leading to increased persistence of La Niña. The delayed thermocline feedback  $b$  also shows less effective damping rates  $b$  as La Niña events become stronger (Fig. 5b), and could also make strong La Niña events last longer. We use the NDO to perform a series of simulations with the objective of isolating the processes responsible for the multiyear persistence of La Niña. First, we estimate linear feedback functions by fitting the heat budget terms following the procedure outlined in appendix B but using linear functions of  $T'$  and  $T'(t - t_0)$  instead of exponentials. Then we perform a series of NDO simulations with different combinations of linear and nonlinear feedback functions.

The simulations show that the NDO is unable to simulate 2-yr La Niña events when all feedbacks are linear but also when the  $a$  and  $c$  functions are *nonlinear* (and the  $b$  function is linear; Fig. 7; yellow, purple, and blue bars). This suggests that the nonlinearities in the Bjerknes feedback and in the atmospheric damping do not play a role in the persistence of La Niña. In contrast, only when the  $b$  function is *nonlinear*, the NDO simulates La Niña events lasting 2 yr in about the same proportion as in CCSM4 (Fig. 7, green bars). This behavior is related to the weaker damping rates for strong La Niña [Fig. 5b,  $T'(t - t_0) \ll 0$ ]. Because the negative delayed thermocline feedback does not increase proportionally with the strength of La Niña, these events have to sit longer in order for the weaker

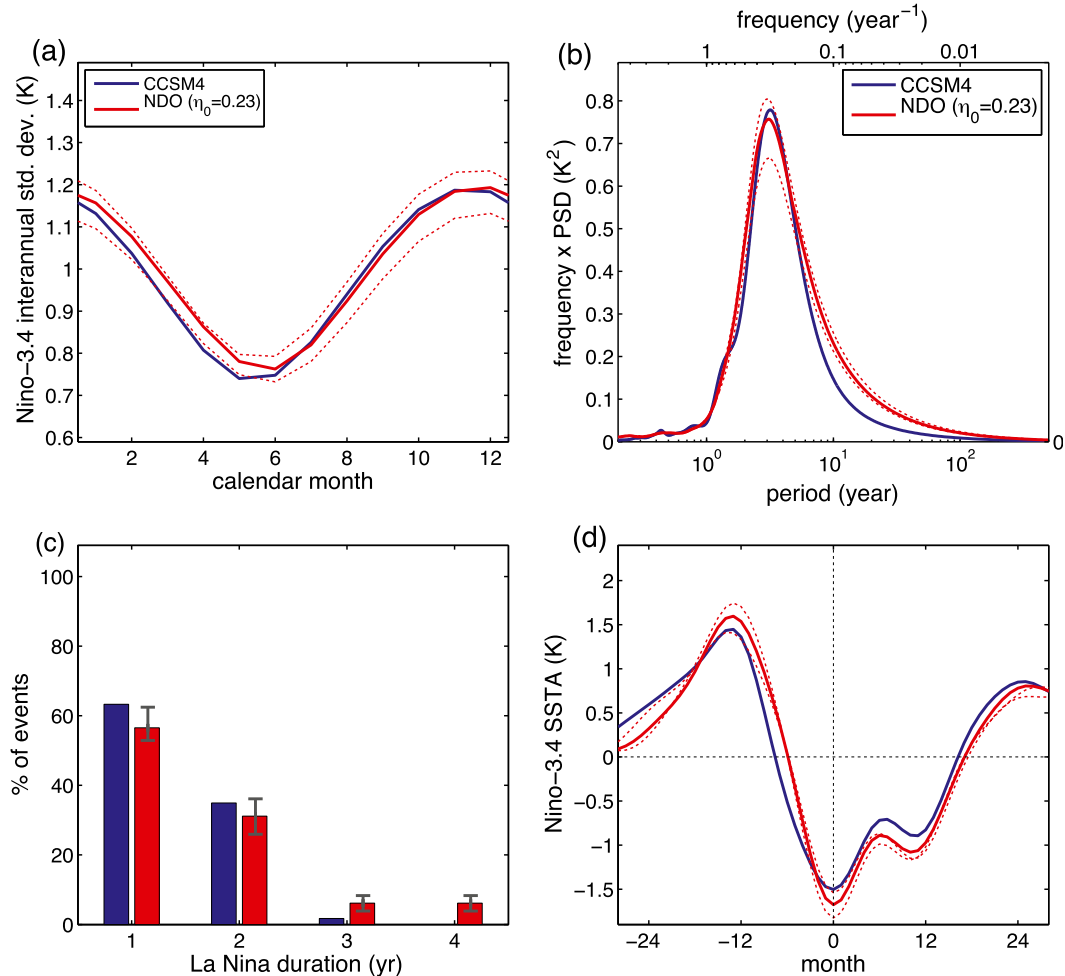


FIG. 6. Niño-3.4 metrics simulated by the NDO (red) compared with the CCSM4 preindustrial control simulation (blue). (a) Seasonal dependence of the standard deviation, (b) spectrum, (c) duration of La Niña events, and (d) composite evolution of 2-yr La Niña events. The NDO metrics are computed from an ensemble of 20 of the 1300-yr-long simulations with  $\eta_0 = 0.23 \text{ K month}^{-1}$  that match the standard deviation of the CCSM4 Niño-3.4 index. Dotted lines indicate the minimum-maximum range estimated from the ensemble.

damping rates to drive SSTs back to neutral conditions. This mechanism allows La Niña events to persist beyond boreal winter into spring, and are thus amplified during late summer/early fall when the total ENSO growth rate returns to positive values (Fig. 5e).

The spectrum of NDO variability also appears to be remarkably sensitive to the nonlinearity of the delayed thermocline feedback. Linear  $b$  reduces the ENSO period from 3 to about 2 yr (Fig. 8, yellow line), while nonlinear  $b$  increases the period to 5 yr (Fig. 8, green line). The increased ENSO period could result from the persistence of La Niña; however, it could be also related to the initiation of El Niño, which is also governed by the thermocline nonlinearity. In other words, after La Niña, the weaker  $b$  damping rates associated with  $T'(t - t_0) < 0$  (Fig. 5b) reduce La Niña's ability to trigger a subsequent El Niño,

resulting in a longer interval between ENSO phases. This lengthening of the ENSO period due to a weaker delayed thermocline response is easily understood in the framework of the J97 recharge oscillator. The  $-bT'(t - t_0)$  term of our NDO is equivalent to the RO's  $\gamma h_w$  term, which governs the frequency of the recharge-discharge oscillation. An increase in  $\gamma$  results in a decrease in the frequency (longer period) of the ENSO oscillation. Therefore, a weakening of this term—in a nonlinear sense—can result in a longer ENSO period.

## 6. Delayed thermocline feedback nonlinearity

### a. Nonlinear processes

What are the physical processes that prevent the delayed thermocline response from increasing proportionally with

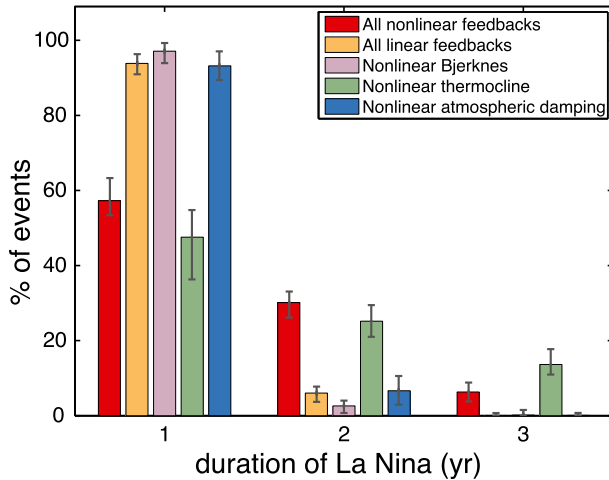


FIG. 7. Duration of La Niña events simulated by the NDO for different combinations of linear and nonlinear feedbacks as indicated in the legend. Colored bars show the mean values from the ensemble of 20 realizations and the error bars show the minimum–maximum range.

the magnitude of La Niña? Our analysis of the nonlinearities in the heat budget showed that the magnitude of  $Q'_{tc}$  quickly saturates as La Niña events become stronger [Fig. 4,  $T'(t - t_0) \ll 0$ ]. Thus, the nonlinearity of the delayed thermocline feedback must result from any of the physical processes linking  $Q'_{tc}$  with  $T'(t - t_0)$ :

- (i) the response of the trade winds to SST anomalies,
- (ii) the delayed response of the thermocline to changes in the trade winds, and
- (iii) the effect of changes in the depth of the thermocline and the thermal stratification at the base of the mixed layer.

These processes link the SST anomalies at the peak of La Niña [ $T'(t - t_0)$ ] with the anomalous advection of the vertical temperature gradient by climatological upwelling ( $Q'_{tc}$ ) 6 months later, which represents a tendency opposing the initial SST anomaly, thus closing the negative feedback loop.

We explored the relationships among these variables in both CCSM4 and reanalysis data in order to determine which of the processes are responsible for the nonlinearity in the delayed thermocline feedback and, hence, the multiyear persistence of La Niña. The response of the trade winds—measured by the anomalies in zonal wind stress averaged over the Niño-3.4 region ( $\tau'^x$ )—exhibits a marked nonlinear behavior in both CCSM4 preindustrial simulation (Fig. 9a) and the ORAS4 data (Fig. 9e). In both the simulated and the reanalysis data, El Niño events exhibit larger zonal wind stress anomalies than La Niña events for SST anomalies

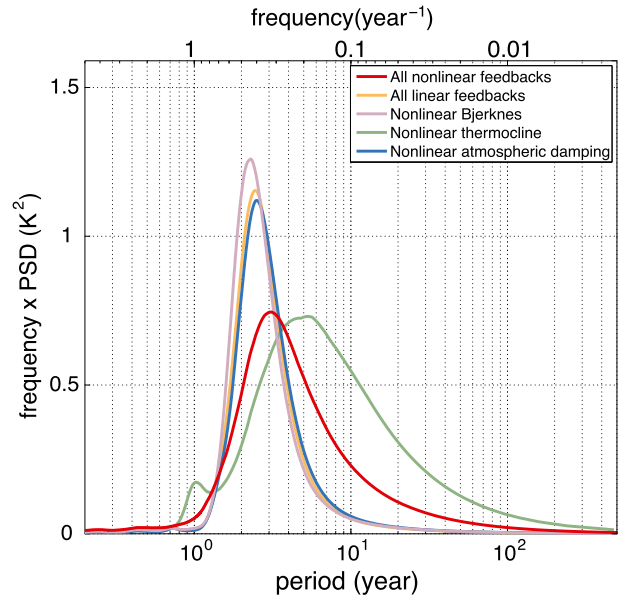


FIG. 8. Ensemble-mean  $T'$  spectra simulated by the NDO for different combinations of linear and nonlinear feedback functions as indicated in the legend.

of the same magnitude. This wind–SST nonlinearity has been linked to the effect of background SST on the convective response of the tropical atmosphere (Hoerling et al. 1997) and invoked to explain asymmetries between the amplitude of El Niño and La Niña (Kang and Kug 2002) and also in their duration (Okumura et al. 2011; Choi et al. 2013; Dommenges et al. 2013).

The delayed response of the thermocline—measured by the depth of thermocline averaged along the equatorial waveguide ( $Z'_{tc}$ )—appears to be *linearly* related to the lagged wind anomalies [ $\tau'^x(t - t_0)$ ] in both CCSM4 (Fig. 9b) and ORAS4 (Fig. 9f). This linear relationship is consistent with linear wave theory, which accurately explains the adjustment of the equatorial ocean to changes in the trade winds in climate models and observations (Yu and McPhaden 1999). Thus, the nonlinearity of the delayed thermocline feedback does not appear to be caused by the response of the depth of the thermocline to changes in the trade winds.

Nonlinear behavior could also arise from the coupling of the thermocline and the mixed layer. The response of the stratification at the base of the mixed layer—measured by the temperature difference between the surface and at a depth of 100 m ( $\Delta T'_{sub}$ )—exhibits a marked asymmetry between El Niño and La Niña both in CCSM4 (Fig. 9c) and in ORAS4 (Fig. 9g). Because La Niña events have a weaker stratification response than El Niño events of the same magnitude, this nonlinearity

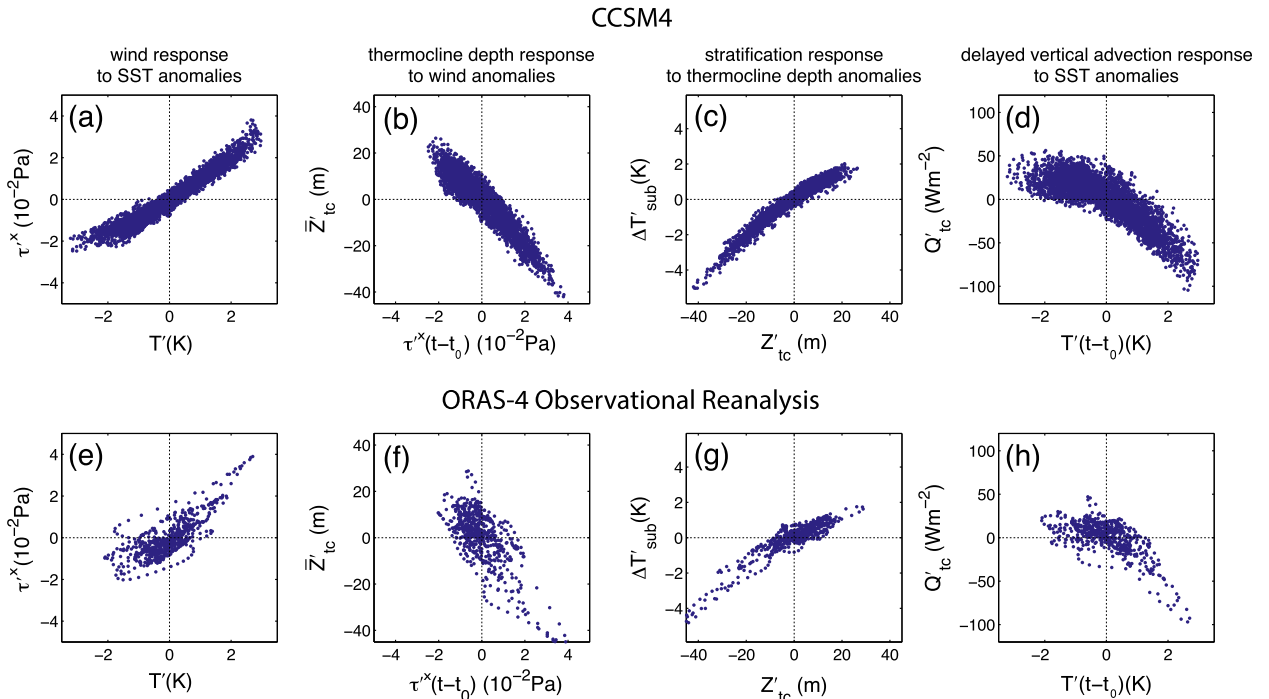


FIG. 9. Processes involved in the delayed thermocline feedback in the (top) CCSM4 and (bottom) ORAS4. (a),(e) Scatterplot between the zonal wind stress anomalies ( $\tau^x$ ) (y axis) and the sea surface temperature anomalies ( $T'$ ) (x axis). (b),(f) Scatterplot between the zonal-mean thermocline depth anomalies ( $\bar{Z}'_{tc}$ ) (y axis) and the lagged zonal wind stress anomalies [ $\tau^x(t - t_0)$ ] (y axis). (c),(g) Scatterplot between the subsurface temperature contrast anomalies ( $\Delta T'_{sub}$ ) (y axis) and the thermocline depth anomalies ( $Z'_{tc}$ ) (x axis). (d),(h) Scatterplot between the advection of the anomalous vertical temperature gradient by climatological upwelling ( $Q'_{tc}$ ) (y axis) and the lagged sea surface temperature anomalies [ $T'(t - t_0)$ ] (x axis). All variables are averaged over the Niño-3.4 region, with the exception of  $\bar{Z}'_{tc}$ , which is zonally averaged across the equatorial Pacific as described in section 2e. Reanalysis data are from ORAS4 (Balmaseda et al. 2013) for the 1960–2011 period.

could also lead to a less effective delayed thermocline feedback. Moreover, the fact that  $\Delta T'_{sub}$  never exceeds 2 K in both CCSM4 and the reanalysis data is highly suggestive that there could be a limit for the magnitude of  $\Delta T'_{sub}$  that a *locally* deeper thermocline anomaly can drive (Figs. 9c,g;  $\bar{Z}'_{tc} > 0$ ). Note that we use the Niño-3.4 averaged  $\bar{Z}'_{tc}$  instead of the  $Z'_{tc}$ ; however, these two variables are in phase and highly correlated due to the fact that the Niño-3.4 region straddles the nodal line of the thermocline tilt, therefore capturing mainly zonal-mean variations in the depth of the thermocline (not shown). In the next subsection, we explore the dynamics of this response in more detail.

### b. Thermocline–SST coupling

Coupling between *local* variations in the depths of the thermocline and the mixed layer is one of the key processes responsible for the nonlinearity of the delayed thermocline feedbacks. The evolution of subsurface temperature anomalies shows key differences in this relationship for 1-yr and 2-yr La Niña events. In both cases, subsurface temperature anomalies associated with

thermocline depth variations (i.e., equatorial heat content) lead the transition from El Niño to La Niña (Figs. 10a,c). These displacements of the thermocline are accompanied by stratification anomalies at the base of the mixed layer: for example, when the thermocline deepens, the stratification at the base of the mixed layer is weaker (Figs. 10b,d).

That 1-yr and 2-yr events exhibit stratification anomalies of the same magnitude is also suggestive that there is a limit to how effective the delayed thermocline feedback is. After the peak of the 1-yr La Niña, the reduced stratification associated with a deeper thermocline still influences the mixed layer (Fig. 10b,  $0 < \text{month} < 6$ ). The associated anomalous vertical advection drives a positive temperature tendency that contributes to the demise of the event. A similar response occurs after the peak of the 2-yr La Niña; however, the reduction in stratification has the same (or even smaller) magnitude than for 1-yr events (Fig. 10d,  $0 < \text{month} < 6$ ). For 2-yr LN, the ability of the deeper thermocline anomalies to influence the stratification at the base of the mixed layer does not increase further than for 1-yr LN (e.g., Fig. 2b).

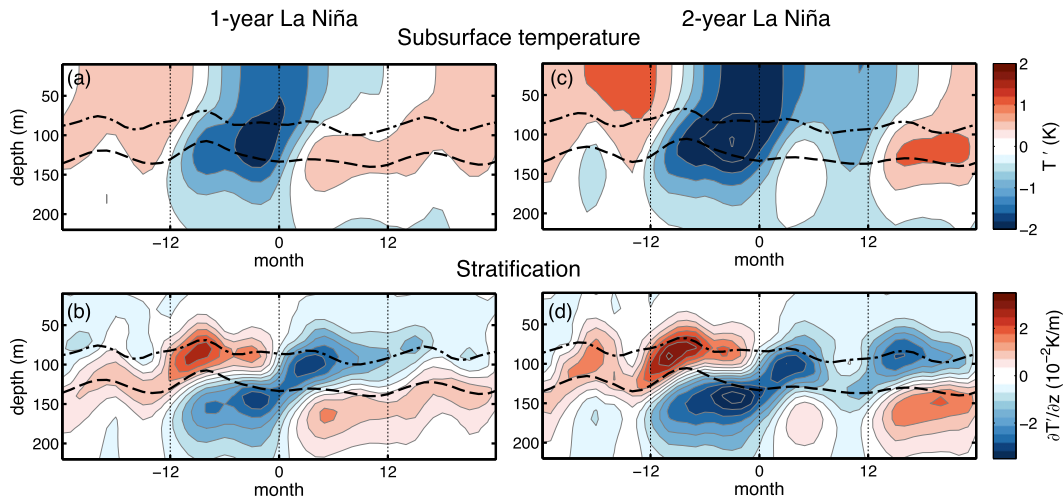


FIG. 10. Composite evolution of (top) subsurface temperature and (bottom) stratification anomalies averaged over the Niño-3.4 region for (left) 1-yr and (right) 2-yr La Niña events. The dashed–dotted line is the depth of mixed layer computed as the depth where temperature is 0.5 K less than that at the surface. The dashed line is the depth of the thermocline, as defined in section 2d.

In order for the delayed thermocline feedback to terminate La Niña in one year, the magnitude of these reduced stratification anomalies should increase linearly with the magnitude of the SST anomalies. However, owing to this limit on the thermocline’s ability to influence the stratification anomalies at the base of the mixed layer, a second year with deeper thermocline anomalies is required for a strong La Niña to return to neutral.

This limit appears to arise from the interaction of the thermocline with the mixed layer. The mixed layer depth (MLD) and thermocline depth ( $Z'_{tc}$ ) are governed by different processes leading to the asymmetry in the  $\Delta T'_{sub} - Z'_{tc}$  response. The MLD is determined by local turbulent and heat fluxes at the sea surface, while  $Z'_{tc}$  is driven by local and remote wind forcing (Cane and Zebiak 1985; Wyrski 1985; Zebiak 1989). This could result in asymmetries in their coupling when the thermocline shoals or deepens. For instance, shoaling of the thermocline is able to drive large  $\Delta T'_{sub}$  because it effectively entrains cold thermocline waters into the mixed layer. This effect is not limited—in fact, it becomes more pronounced—as the thermocline shoals. In contrast, deepening of the thermocline *decouples* the thermocline waters from the mixed layer. That is, a deeper  $Z'_{tc}$  becomes increasingly ineffective at detraining cold waters from the mixed layer. This mechanism appears to be responsible for the nonlinear coupling between  $\Delta T'_{sub}$  and  $Z'_{tc}$  shown in Figs. 9 and 10. This nonlinearity only occurs in the central Pacific—both in CCSM4 and in nature—because this is the region where the climatological MLD is shallower than the

thermocline. The dependence of  $\Delta T'_{sub}$  on  $Z'_{tc}$  becomes linear toward the eastern Pacific as the thermocline and the mixed layer merge.

The model of Zebiak and Cane (1987, hereafter ZC87) implements a parameterization for the temperature of the entrained water that leads to a similar nonlinearity between  $\Delta T'_{sub}$  and  $Z'_{tc}$ . In this parameterization, however, the effect of a deeper or shallower  $Z'_{tc}$  on  $\Delta T'_{sub}$  is symmetric, and both cases saturate as  $Z'_{tc}$  become too shallow or too deep. This nonlinearity acts as nonlinear damping in the ZC87 model, keeping ENSO events from growing indefinitely. Furthermore, in the ZC87 model the nonlinearity is more pronounced in the eastern equatorial Pacific, and only very large events enter the nonlinear regime. In contrast, most La Niña events may operate in the nonlinear regime in CCSM4 and nature, as shown by the pronounced flattening of the  $\Delta T'_{sub} - Z'_{tc}$  dependence (Figs. 9c,g).

## 7. Discussion

### a. Nonlinear controls on the multiyear persistence of La Niña

We identified two nonlinear processes controlling the multiyear duration of La Niña: 1) the response of the equatorial trade winds to SST anomalies and 2) the effect of changes in the depth of thermocline on the stratification at the base of the mixed layer. Previous studies have focused on the first process, showing that a realistic wind–SST nonlinearity is capable of producing

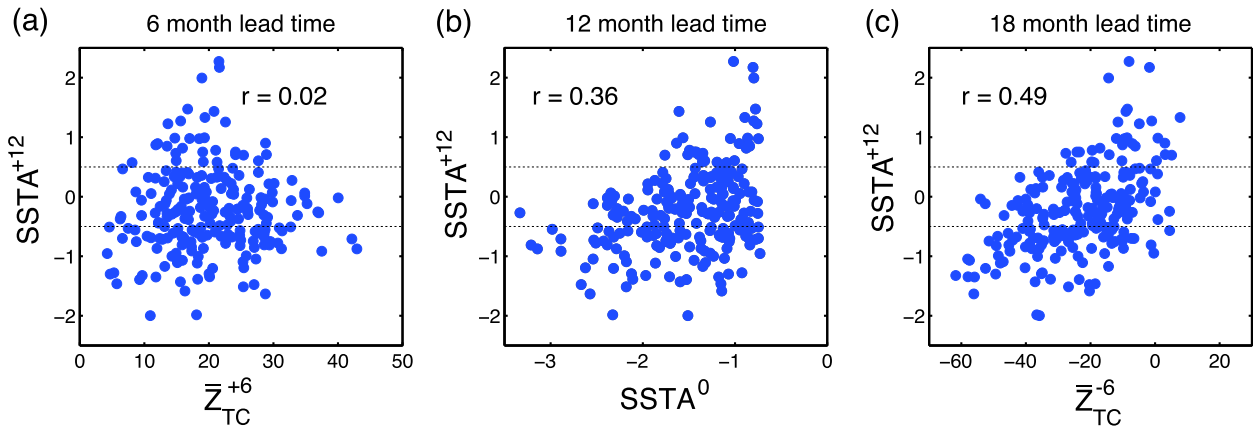


FIG. 11. Scatterplots showing the relationship between, on the y axis, Niño-3.4 SST anomalies 12 months after the first-year peak of La Niña ( $SSTA^{+12}$ ) and, on the x axis, (a) zonally averaged thermocline depth anomalies 6 months prior ( $Z_{TC}^{+6}$ ), (b) Niño-3.4 SST anomalies 12 months prior ( $SSTA^0$ ), i.e., at the first-year peak of La Niña, and (c) zonally averaged thermocline depth anomalies 18 months prior ( $Z_{TC}^{-6}$ ). Both La Niña events lasting 1 yr ( $SSTA^{+12} > -0.5$  K) and 2 yr or longer ( $SSTA^{+12} < -0.5$  K) are shown. The correlation coefficient  $r$  between the two variables is indicated in each panel.

persistent La Niña events (Okumura et al. 2011; Choi et al. 2013; Dommenges et al. 2013); however, they also conclude that this nonlinearity alone does not produce as many persistent La Niña events as observed (Choi et al. 2013). Similarly, 2-yr La Niña events are not as common as in CCSM4 in the model of Dommenges et al. (2013). This can be seen in their Fig. 11b, which does not show a clear La Niña signal during the second year, in contrast to the composite derived from observations and CCSM4 (Fig. 1).

Our results show that the second process—the thermocline nonlinearity—is also required to simulate the correct proportion of 2-yr La Niña events. Munnich et al. (1991) also found that cold events last longer when a similar piecewise nonlinearity is included in their ENSO model. Reanalysis data also show evidence for the thermocline nonlinearity (Fig. 9g), which, combined with the wind–SST nonlinearity (Fig. 9e), lead to a highly nonlinear  $Q'_{TC}$  (Fig. 9h), the key term contributing to the delayed thermocline feedback. Therefore, it is very likely that both nonlinearities play a key role in the occurrence of 2-yr La Niña events in nature.

### b. ENSO period

The origin of the rather long ENSO period compared with the time scale of the thermocline adjustment has been a matter of debate (e.g., Schopf and Suarez 1990; J97). Our NDO simulations show that, in the stable regime, the thermocline nonlinearity has a direct impact on ENSO period by lengthening and broadening it. This process offers an alternative explanation for these characteristics of the observed ENSO. The persistence

of La Niña events would also affect the power spectrum of ENSO. However, the thermocline nonlinearity could also have an influence on the initiation of El Niño events, having an effect on how often they occur. Positive  $Z'_{TC}$  also leads the initiation of El Niño events; therefore, the saturation of  $\Delta T'_{sub}$  for large positive  $Z'_{TC}$  could also be disfavoring the triggering of El Niño events. Because our NDO is in the stable regime, we do not find evidence for chaos-induced period doubling as found by other studies using similar simple models (Munnich et al. 1991). However, given that ENSO appears to operate in a nearly stable regime (Penland and Sardeshmukh 1995; Thompson and Battisti 2001), our results suggest that the thermocline nonlinearity could be contributing to the rather long ENSO period observed in nature.

### c. Precursors

Based on the dynamical understanding presented above, we have begun to explore precursors for the return of La Niña in the second year. Heat content anomalies associated with variations in the depth of the thermocline are typically indicative of future SST anomalies with a lead time of 2–3 seasons. However, the depth of thermocline 6 months after the first peak of La Niña does not appear to be correlated with SST anomalies ( $r = 0.02$ ) in the second year (Fig. 11a). In contrast, the magnitude of the negative SST anomalies during the first year of La Niña exhibits a larger correlation with the SST anomalies ( $r = 0.36$ ) in the second year (Fig. 11b). This is consistent with the idea that a stronger La Niña will tend to persist longer than a weaker one (Hu et al. 2013). Our dynamical analysis

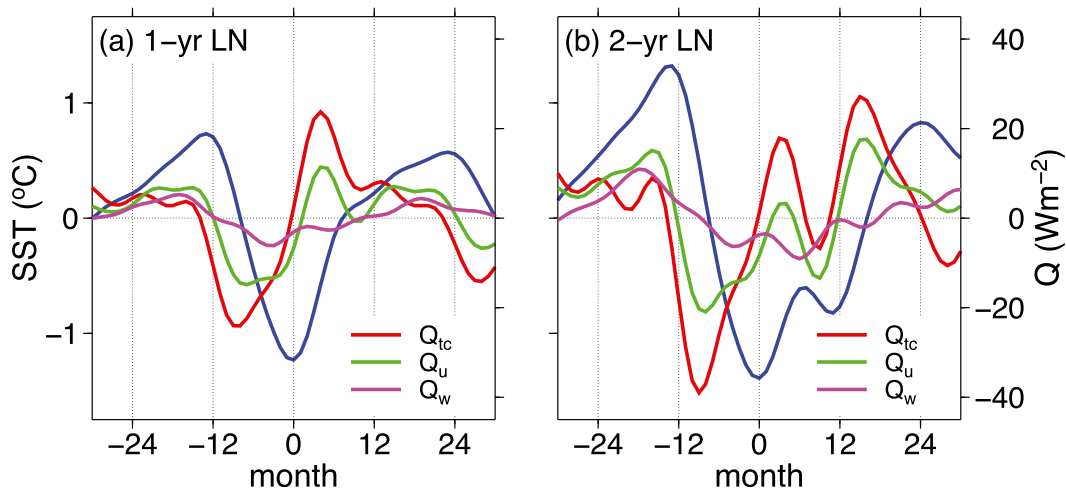


FIG. A1. Composite of thermocline ( $Q'_{tc}$ ; red), zonal advection ( $Q'_u$ ; green), and upwelling ( $Q'_w$ ; magenta) terms of the linearized heat budget for (a) 1-yr and (b) 2-yr La Niña events simulated by CCSM4. Month 0 coincides with the first-year peak of La Niña. The sea surface temperature anomalies and the heat budget term are averaged over the Niño-3.4 region ( $5^{\circ}\text{S}$ – $5^{\circ}\text{N}$ ,  $120^{\circ}$ – $170^{\circ}\text{W}$ ). Further details on the methodology to compute anomalies and select 1-yr and 2-yr La Niña events may be found in section 2.

indicates that the rate at which heat content is replenished is the main factor governing the duration of La Niña. For this reason, we looked at the depth of the thermocline 6 months before the first peak of La Niña, and found that it exhibits an even larger correlation with SST anomalies ( $r = 0.49$ ) in the second year (Fig. 11c). This could provide an 18-month lead time for predicting the return of La Niña. A more systematic study using “perfect model” prediction experiments is needed to explore the precursors of 2-yr La Niña beyond this preliminary analysis.

## 8. Conclusions

We developed a nonlinear delayed oscillator (NDO) based on the model of SS88 and BH89. The NDO features nonlinear and seasonally dependent ENSO feedbacks derived from the CCSM4 heat budget. Despite its simplicity, the NDO simulates many features in quantitative agreement with the CCSM4 ENSO, such as the positive skewness, seasonal modulation of variance, a broad peaked spectrum centered at a period of 3–4 yr, and a  $\sim 35\%$  frequency of occurrence of 2-yr La Niña events.

Simulations with the NDO reveal that a nonlinearity in the delayed thermocline feedback is responsible for the multiyear persistence of La Niña. This nonlinearity is due to the dependence of the subsurface temperature gradient  $\Delta T'_{\text{sub}}$  on  $Z'_{\text{tc}}$ , which leads to a less effective delayed thermocline-driven termination of La Niña events. Nonlinearities in other processes, such as

the response of winds to SST anomalies, could also increase the duration of La Niña as proposed by previous studies (Choi et al. 2013; Dommenges et al. 2013); however, our analysis shows that the  $\Delta T'_{\text{sub}} - Z'_{\text{tc}}$  nonlinearity is required to explain the large fraction (35%) of 2-yr LN events simulated by CCSM4. Furthermore, the thermocline nonlinearity has a direct effect on the spectral properties of ENSO resulting in a broader and longer period. This process appears to operate in nature as well; however, its precise role on the observed multiyear persistence of La Niña or, more generally, on ENSO’s period requires further research.

Finally, the predictability of the termination of La Niña events cannot be quantified from our analysis. On one hand, the predictability should be rather low because of the weaker delayed thermocline feedback. On the other hand, whether the ENSO system remains in the linear regime or enters the nonlinear regime could be indicative of whether La Niña will be effectively terminated or not. Last, heat content anomalies, which are typically interpreted as precursors of El Niño or La Niña conditions, are not indicative of the return of La Niña in the second year. However, our results indicate that the depth of the thermocline 6 months before the first-year La Niña could be a more accurate precursor for the persistence of La Niña. This relationship could provide a prediction of the duration of La Niña with an 18-month lead time. Owing to its disproportionate impact on drought throughout the world, further research on the predictability and prediction of the duration of

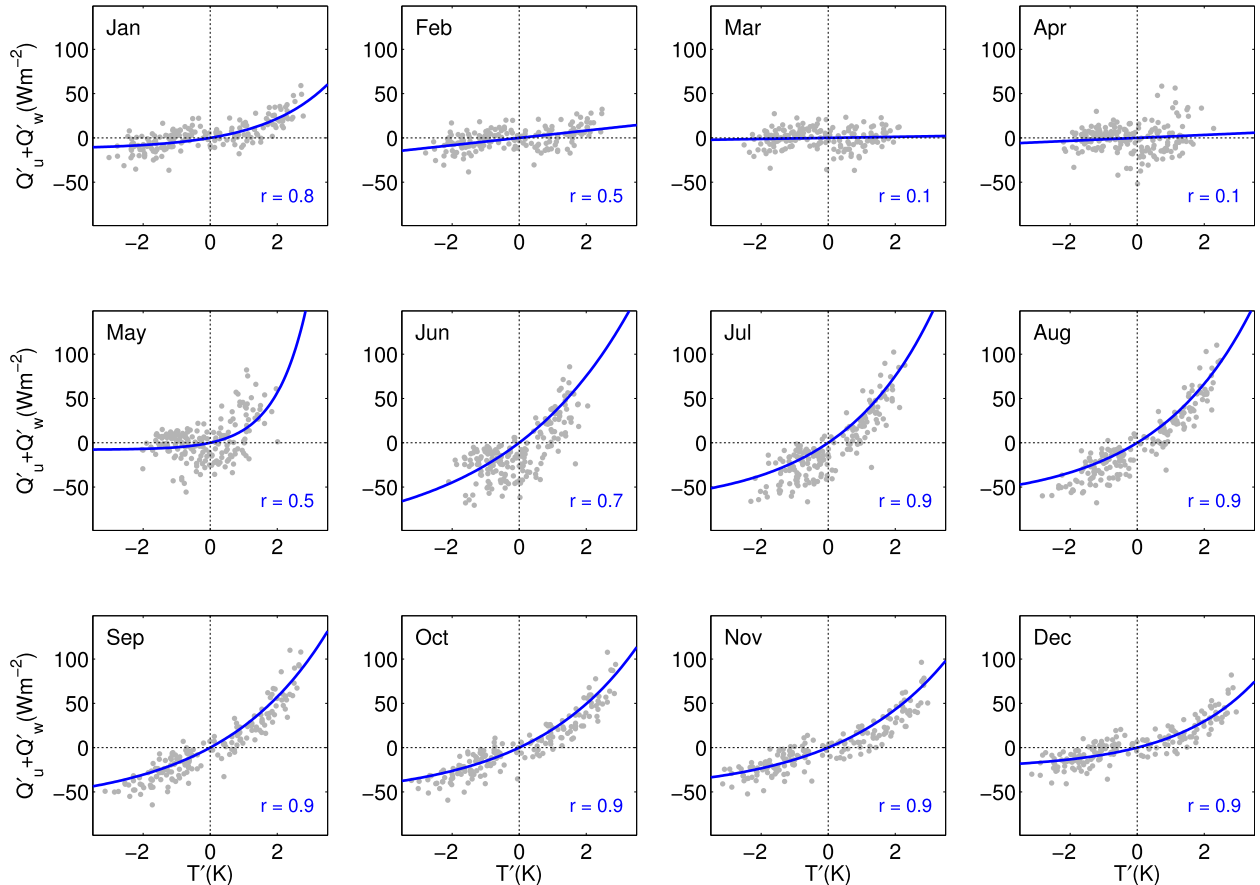


FIG. B1. Scatterplot for each calendar month (gray dots) between the sum of the advection by zonal velocity anomalies ( $Q'_u$ ) and by vertical velocity anomalies ( $Q'_w$ ) (y axis) and the sea surface temperature anomalies ( $T'$ ) (x axis) averaged over the Niño-3.4 region. The blue curves are the best-fit exponential functions derived following the methodology described in appendix B. The correlation coefficient  $r$  between the two variables is indicated in each panel.

La Niña events could result in concrete and direct societal benefits.

*Acknowledgments.* We thank Axel Timmerman, Karl Stein, Yuko Okumura, Amy Clement, and three anonymous reviewers for constructive comments that helped improved the clarity and quality of the manuscript. PDN was supported by the SOEST Young Investigator Fellowship of the University of Hawai'i. This study was supported by NOAA's Climate Program Office's Modeling, Analysis, Predictions, and Projections program (Grant NA14OAR4310229). Computing resources were provided by the Climate Simulation Laboratory at NCAR's Computational and Information Systems Laboratory (CISL), sponsored by the National Science Foundation and other agencies. This research was supported by the Japan Agency for Marine-Earth Science and Technology (JAMSTEC); by NASA through Grant NNX07AG53G; and by NOAA through Grant

NA11NMF4320128, which sponsors research at the International Pacific Research Center.

## APPENDIX A

### Composite Heat Budget Analysis

We decomposed the temperature advection by ocean currents into the different linear and nonlinear terms in order to explore role of ocean dynamics on the onset, persistence, and decay of La Niña events simulated by CCSM4. Only the following terms are important on interannual time scales:

$$Q'_u = -\rho_0 c_p \int_{-H}^0 u' \frac{\partial \bar{T}}{\partial x} dz, \quad (\text{A1a})$$

$$Q'_{tc} = -\rho_0 c_p \int_{-H}^0 \bar{w}' \frac{\partial T'}{\partial z} dz, \quad (\text{A1b})$$

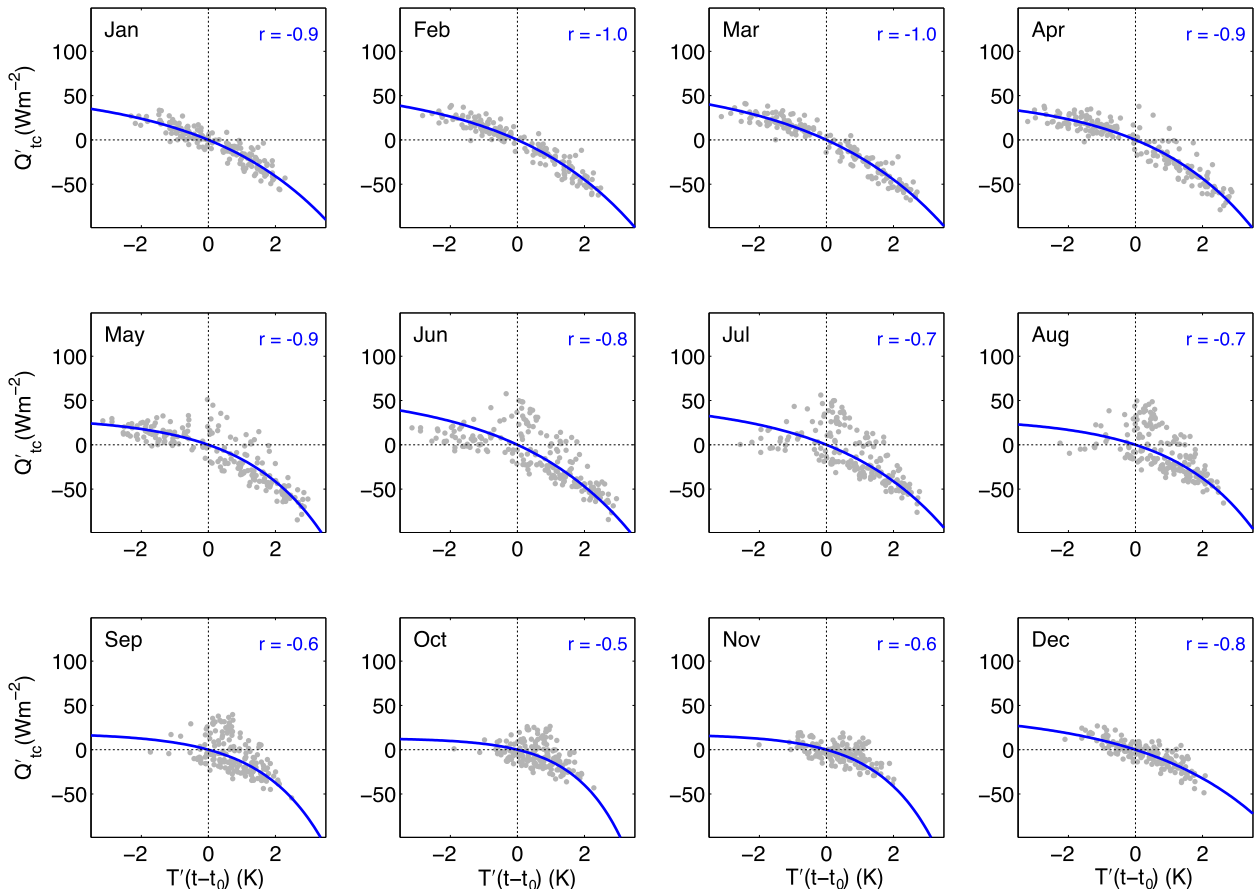


FIG. B2. Scatterplot for each calendar month (gray dots) between the vertical advection by thermocline anomalies ( $Q'_{tc}$ ) (y axis) and the lagged sea surface temperature anomalies [ $T'(t - t_0)$ ] (x axis) averaged over the Niño-3.4 region. The blue curves are the best-fit exponential functions derived following the methodology described in appendix B. The correlation coefficient  $r$  between the two variables is indicated in each panel.

$$Q'_w = -\rho_0 c_p \int_{-H}^0 w' \frac{\partial \bar{T}}{\partial z} dz, \quad \text{and} \quad (\text{A1c})$$

$$Q'_{nl} = -\rho_0 c_p \int_{-H}^0 u' \frac{\partial T'}{\partial x} dz, \quad (\text{A1d})$$

where primed quantities are anomalies with respect to the seasonal cycle (bar quantities),  $\rho_0 c_p = 4.1 \times 10^6 \text{ J m}^{-3} \text{ K}^{-1}$  is the ocean density times the specific heat of seawater, and  $H = 100 \text{ m}$ . The rationale for using  $H = 100 \text{ m}$  is extensively discussed in section 2f. Furthermore, while being energetically consistent, integrating the advection terms (A1) over a constant depth layer poses limitations to fully describe the influence of some of the processes. Using a spatially constant depth could fail to capture the changes involving the thermocline because of its east–west tilt. For instance, the anomalous stratification associated with the deepening of the thermocline driven by La Niña does not occur on a constant depth surface and

follows the east–west tilt of the climatological thermocline instead. We explored the vertical dependence of these terms and found that temperature tendencies associated with changes in thermocline, zonal currents, and upwelling do not depend strongly when  $90 \text{ m} \leq H \leq 110 \text{ m}$ .

The composite heat budget of 1-yr LN and 2-yr LN events shows that  $Q'_{tc}$  [see (A1b)], the advection of temperature anomalies by climatological upwelling, and  $Q'_u$  [see (A1a)], the temperature advection by zonal current anomalies, lead the development of SST anomalies (Fig. A1, red and green lines, respectively). The evolution of  $Q'_{tc}$  is highly correlated with that of  $Z'_{tc}$  through the entire ENSO cycle. This occurs because changes in the depth of thermocline drive changes in stratification  $\partial T'/\partial z$ , altering the temperature advection by climatological upwelling  $Q'_{tc}$ . Because of this close relationship with  $Z'_{tc}$ , the  $Q'_{tc}$  term can be equated to the delayed thermocline feedback of the SS88 and BH89 delayed oscillator or the recharge

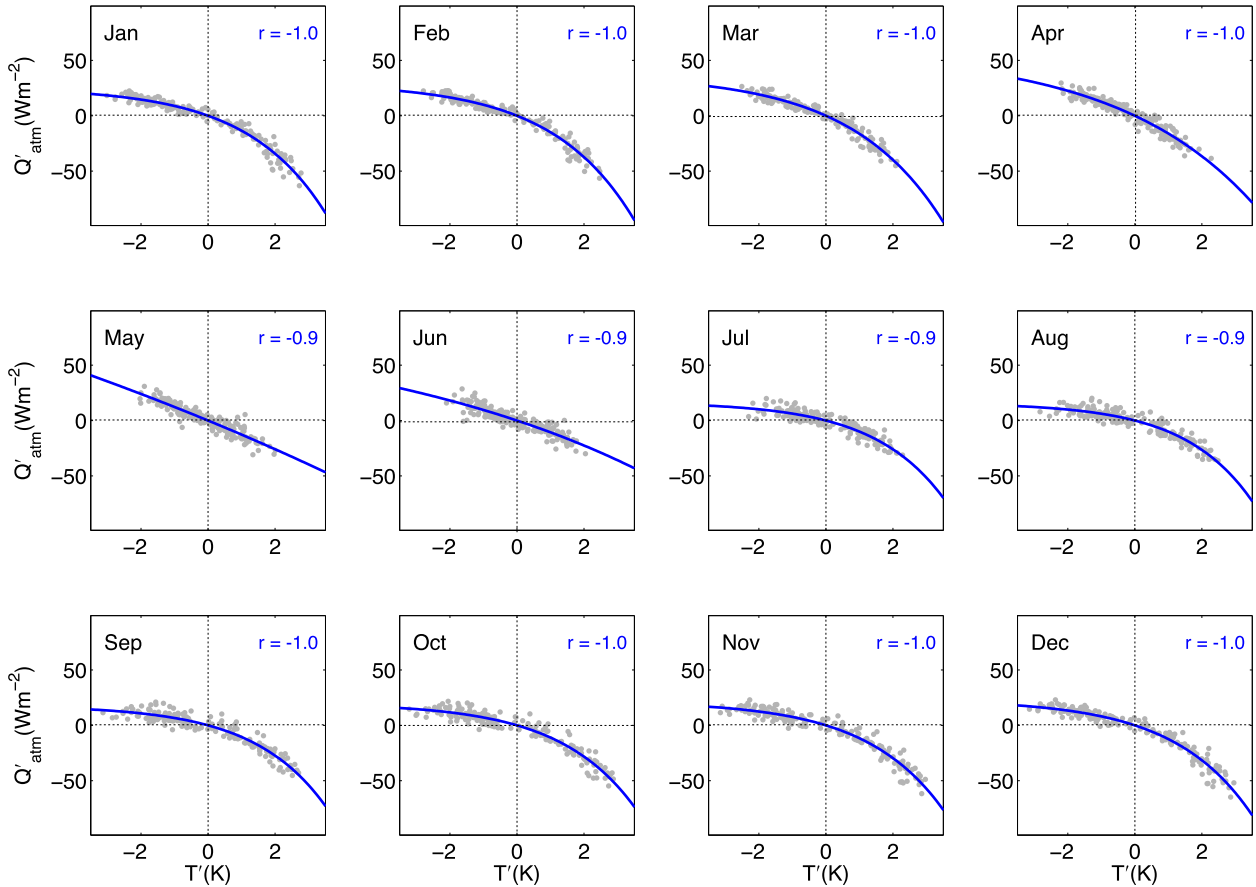


FIG. B3. Scatterplot for each calendar month (gray dots) between the air–sea flux anomalies ( $Q'_{\text{atm}}$ ) (y axis) and the sea surface temperature anomalies [ $T'(t - t_0)$ ] (x axis) averaged over the Niño-3.4 region. The blue curves are the best-fit exponential functions derived following the methodology described in appendix B. The correlation coefficient  $r$  between the two variables is indicated in each panel.

term of J97's recharge oscillator. The evolution of these terms, in particular  $Q'_{\text{tc}}$ , shows that delayed thermocline anomalies play a key role throughout the entire ENSO cycle, consistent with the dynamics of simple linear models of ENSO, such as the DO and the RO. The advection of the climatological temperature gradient by upwelling anomalies  $Q'_w$  [see (A1c)] is in phase with SST anomalies throughout the entire ENSO cycle (Fig. A1, purple line), thus acting as a positive feedback. The evolution of this term is consistent with the positive feedback proposed by Bjerknes (1969) in which proposed that wind-driven changes in upwelling,  $w'$ , play a key role in the growth of El Niño.

The advection terms for 2-yr LN events exhibit departures from oscillatory dynamics similar to those seen in evolution of the thermocline (Fig. 2). The heat budget composite shows that  $Q'_{\text{tc}}$  leads SST anomalies during the transition from El Niño to La Niña, but after La Niña's first peak the positive tendency associated

with  $Q'_{\text{tc}}$  is not sufficient to return SST anomalies to neutral and they remain negative (Fig. A1b, red line). Note that, after the first year of La Niña, the positive  $Q'_{\text{tc}}$  and  $Q'_u$  anomalies are larger for 1-yr events (Fig. A1a) than for 2-yr events (Fig. A1b), even though the SST anomalies are about the same magnitude or even smaller.

Note that the evolution of  $Q'_u$  is not always in quadrature with SST anomalies during both 1-yr and 2-yr events. The development of El Niño and La Niña is characterized by  $Q'_u$  in phase with SST anomalies, while the transition from El Niño to La Niña is characterized by  $Q'_u$  in quadrature with SST anomalies (Figs. A1a,b, green line). These differences arise because the zonal current anomaly  $u'$  comprises a wind-driven component—a direct response to the wind anomalies—and a Kelvin wave component—associated with the delayed thermocline response (Jin et al. 2006). The  $Q'_u$  variability correlated with SST anomalies contributes to the positive Bjerknes

feedback (in the same way than  $Q'_w$ ), while the variability in quadrature contributes to the delayed thermocline feedback.

## APPENDIX B

### Derivation of Feedback Functions

We derive the  $a$ ,  $b$ ,  $c$ , and  $d$  functions of the NDO (2) by fitting the terms of the heat budget (1) to the following functions:

$$\hat{Q}_u(T') = C_1 e^{C_2 T'} + C_3 e^{C_4 T'(t-t_0)} + C_5, \quad (\text{B1a})$$

$$\hat{Q}_{tc}(T') = C_1 e^{C_2 T'} + C_3 e^{C_4 T'(t-t_0)} + C_5, \quad (\text{B1b})$$

$$\hat{Q}_w(T') = C_1 e^{C_2 T'} + C_3, \quad (\text{B1c})$$

$$\hat{Q}_{nl}(T') = C_1 e^{C_2 T'} + C_3, \quad \text{and} \quad (\text{B1d})$$

$$\hat{Q}_{atm}(T') = C_1 e^{C_2 T'} + C_3, \quad (\text{B1e})$$

where the constants  $C_n$  are different for each  $\hat{Q}$  function. The only functions exhibiting multiple dependence on  $T'$  and  $T'(t - t_0)$  are  $\hat{Q}_u$  and  $\hat{Q}_{tc}$  since the corresponding terms of the heat budget  $Q'_u$  and  $Q'_{tc}$  exhibit dependence on both Niño-3.4 SST anomalies and on  $\bar{Z}'_{tc}$ .

We estimate the  $C_n$  constants through an iterative least squares estimation as implemented by MATLAB's `nlinfit` function. We perform these regressions using heat budget data for each calendar month in order to isolate the seasonal dependence of the ENSO feedbacks discussed in section 3b. Figures B1–B3 show the data and the best-fit curves for each calendar month. We obtain correlations as high as 1.0 during seasons when each feedback is strongest: September–November (SON) for the Bjerknes feedback (Fig. B1) and April–June (AMJ) for the delayed thermocline feedback (Fig. B2).

We then group together the terms of (4) that depend on  $T'$  and on  $T'(t - t_0)$  to construct the feedback functions of the NDO equation (2). We drop the constant terms of (B1) to ensure that the associated terms of (2) are zero when  $T'$  is zero. We also express these functions in units of kelvins per year, dividing the  $\hat{Q}$  functions (B1) by  $\rho_0 c_p H / 3.1104 \times 10^4 \text{ yr}^{-1}$ . The Bjerknes feedback term  $aT'$  results from combining the  $T'$  terms of  $\hat{Q}_u$  and  $\hat{Q}_{tc}$  with  $\hat{Q}_w$ . The delayed thermocline feedback term,  $-bT'(t - t_0)$ , results from grouping the  $T'(t - t_0)$  terms of  $\hat{Q}_u$  and  $\hat{Q}_{tc}$ . The atmospheric damping term  $-cT'$  is  $\hat{Q}_{atm}(T')$ , while the nonlinear advection term  $-dT$  is  $\hat{Q}_{nl}(T')$ . Last, we divide the resulting functions by either  $T'$  or  $T'(t - t_0)$  to obtain the growth and damping rates  $a$ ,  $b$ ,  $c$ , and  $d$ .

## REFERENCES

- Balmaseda, M. A., K. Mogensen, and A. T. Weaver, 2013: Evaluation of the ECMWF ocean reanalysis system ORAS4. *Quart. J. Roy. Meteor. Soc.*, **139**, 1132–1161, doi:10.1002/qj.2063.
- Battisti, D. S., and A. C. Hirst, 1989: Interannual variability in a tropical atmosphere–ocean model: Influence of the basic state, ocean geometry and nonlinearity. *J. Atmos. Sci.*, **46**, 1687–1712, doi:10.1175/1520-0469(1989)046<1687:IVIATA>2.0.CO;2.
- Bellenger, H., E. Guilyardi, J. Leloup, M. Lengaigne, and J. Vialard, 2014: ENSO representation in climate models: From CMIP3 to CMIP5. *Climate Dyn.*, **42** (7–8), 1999–2018, doi:10.1007/s00382-013-1783-z.
- Bjerknes, J., 1969: Atmospheric teleconnections from the equatorial Pacific. *Mon. Wea. Rev.*, **97**, 163–172, doi:10.1175/1520-0493(1969)097<0163:ATFTEP>2.3.CO;2.
- Burgers, G., F.-F. Jin, and G. J. van Oldenborgh, 2005: The simplest ENSO recharge oscillator. *Geophys. Res. Lett.*, **32**, L13706, doi:10.1029/2005GL022951.
- Cane, M. A., and S. E. Zebiak, 1985: A theory for El Niño and the Southern Oscillation. *Science*, **228**, 1085–1087, doi:10.1126/science.228.4703.1085.
- Capotondi, A., 2013: ENSO diversity in the NCAR CCSM4 climate model. *J. Geophys. Res. Oceans*, **118**, 4755–4770, doi:10.1002/jgrc.20335.
- Choi, K.-Y., G. A. Vecchi, and A. T. Wittenberg, 2013: ENSO transition, duration and amplitude asymmetries: Role of the nonlinear wind stress coupling in a conceptual model. *J. Climate*, **26**, 9462–9476, doi:10.1175/JCLI-D-13-00045.1.
- Deser, C., and Coauthors, 2012: ENSO and Pacific decadal variability in the Community Climate System Model version 4. *J. Climate*, **25**, 2622–2651, doi:10.1175/JCLI-D-11-00301.1.
- DiNezio, P. N., A. C. Clement, G. A. Vecchi, B. J. Soden, B. P. Kirtman, and S.-K. Lee, 2009: Climate response of the equatorial Pacific to global warming. *J. Climate*, **22**, 4873–4892, doi:10.1175/2009JCLI2982.1.
- , B. P. Kirtman, A. C. Clement, S.-K. Lee, G. A. Vecchi, and A. Wittenberg, 2012: Mean climate controls on the simulated response of ENSO to increasing greenhouse gases. *J. Climate*, **25**, 7399–7420, doi:10.1175/JCLI-D-11-00494.1.
- Dommenget, D., T. Bayr, and C. Frauen, 2013: Analysis of the nonlinearity in the pattern and time evolution of El Niño Southern Oscillation. *Climate Dyn.*, **40** (11–12), 2825–2847, doi:10.1007/s00382-012-1475-0.
- , S. Haase, T. Bayr, and C. Frauen, 2014: Analysis of the slab ocean El Niño atmospheric feedbacks in observed and simulated ENSO dynamics. *Climate Dyn.*, **42**, 3187–3205, doi:10.1007/s00382-014-2057-0.
- Eisenman, I., L. Yu, and E. Tziperman, 2005: Westerly wind bursts: ENSO's tail rather than the dog? *J. Climate*, **18**, 5224–5238, doi:10.1175/JCLI3588.1.
- Frauen, C., and D. Dommengot, 2010: El Niño and La Niña amplitude asymmetry caused by atmospheric feedbacks. *Geophys. Res. Lett.*, **37**, L18801, doi:10.1029/2010GL044444.
- Gent, P. R., and Coauthors, 2011: The Community Climate System Model version 4. *J. Climate*, **24**, 4973–4991, doi:10.1175/2011JCLI4083.1.
- Hoerling, M. P., A. Kumar, and M. Zhong, 1997: El Niño, La Niña, and the nonlinearity of their teleconnections. *J. Climate*, **10**, 1769–1786, doi:10.1175/1520-0442(1997)010<1769:ENOLNA>2.0.CO;2.
- Hu, Z.-Z., A. Kumar, Y. Xue, and B. Jha, 2013: Why were some La Niñas followed by another La Niña? *Climate Dyn.*, **42**, 1029–1042, doi:10.1007/s00382-013-1917-3.

- Jin, F.-F., 1997: An equatorial ocean recharge paradigm for ENSO. Part I: Conceptual model. *J. Atmos. Sci.*, **54**, 811–829, doi:10.1175/1520-0469(1997)054<0811:AEORPF>2.0.CO;2.
- , S. T. Kim, and L. Bejarano, 2006: A coupled-stability index for ENSO. *Geophys. Res. Lett.*, **33**, L23708, doi:10.1029/2006GL027221.
- , L. Lin, A. Timmermann, and J. Zhao, 2007: Ensemble-mean dynamics of the ENSO recharge oscillator under state-dependent stochastic forcing. *Geophys. Res. Lett.*, **34**, L03807, doi:10.1029/2006GL027372.
- Kang, I.-S., and J.-S. Kug, 2002: El Niño and La Niña sea surface temperature anomalies: Asymmetry characteristics associated with their wind stress anomalies. *J. Geophys. Res.*, **107**, 4372, doi:10.1029/2001JD000393.
- Kessler, W. S., 2002: Is ENSO a cycle or a series of events? *Geophys. Res. Lett.*, **29**, 2125, doi:10.1029/2002GL015924.
- Kim, S., and F.-F. Jin, 2011: An ENSO stability analysis. Part II: Results from the twentieth and twenty-first century simulations of the CMIP3 models. *Climate Dyn.*, **36** (7–8), 1609–1627, doi:10.1007/s00382-010-0872-5.
- Larkin, N. K., and D. E. Harrison, 2002: ENSO warm (El Niño) and cold (La Niña) event life cycles: Ocean surface anomaly patterns, their symmetries, asymmetries, and implications. *J. Climate*, **15**, 1118–1140, doi:10.1175/1520-0442(2002)015<1118:EWENOA>2.0.CO;2.
- McPhaden, M. J., and X. Yu, 1999: Equatorial waves and the 1997–98 El Niño. *Geophys. Res. Lett.*, **26**, 2961–2964, doi:10.1029/1999GL004901.
- , and X. Zhang, 2009: Asymmetry in zonal phase propagation of ENSO sea surface temperature anomalies. *Geophys. Res. Lett.*, **36**, L13703, doi:10.1029/2009GL038774.
- Munnich, M., M. A. Cane, and S. E. Zebiak, 1991: A Study of self-excited oscillations of the tropical ocean–atmosphere system. Part II: Nonlinear cases. *J. Atmos. Sci.*, **48**, 1238–1248, doi:10.1175/1520-0469(1991)048<1238:ASOSEO>2.0.CO;2.
- Nagura, M., K. Ando, and K. Mizuno, 2008: Pausing of the ENSO cycle: A case study from 1998 to 2002. *J. Climate*, **21**, 342–363, doi:10.1175/2007JCLI1765.1.
- Neale, R. B., J. H. Richter, and M. Jochum, 2008: The impact of convection on ENSO: From a delayed oscillator to a series of events. *J. Climate*, **21**, 5904–5924, doi:10.1175/2008JCLI2244.1.
- Ohba, M., and H. Ueda, 2009: Role of nonlinear atmospheric response to SST on the asymmetric transition process of ENSO. *J. Climate*, **22**, 177–192, doi:10.1175/2008JCLI2334.1.
- , D. Nohara, and H. Ueda, 2010: Simulation of asymmetric ENSO transition in WCRP CMIP3 multimodel experiments. *J. Climate*, **23**, 6051–6067, doi:10.1175/2010JCLI3608.1.
- Okumura, Y. M., and C. Deser, 2010: Asymmetry in the duration of El Niño and La Niña. *J. Climate*, **23**, 5826–5843, doi:10.1175/2010JCLI3592.1.
- , M. Ohba, C. Deser, and H. Ueda, 2011: A proposed mechanism for the asymmetric duration of El Niño and La Niña. *J. Climate*, **24**, 3822–3829, doi:10.1175/2011JCLI3999.1.
- Penland, C., and P. D. Sardeshmukh, 1995: The optimal growth of tropical sea surface temperature anomalies. *J. Climate*, **8**, 1999–2024, doi:10.1175/1520-0442(1995)008<1999:TOGOTS>2.0.CO;2.
- Rayner, N. A., D. E. Parker, E. B. Horton, C. K. Folland, L. V. Alexander, D. P. Rowell, E. C. Kent, and A. Kaplan, 2003: Global analyses of sea surface temperature, sea ice, and night marine air temperature since the late nineteenth century. *J. Geophys. Res.*, **108**, 4407, doi:10.1029/2002JD002670.
- Schopf, P. S., and M. J. Suarez, 1988: Vacillations in a coupled ocean–atmosphere model. *J. Atmos. Sci.*, **45**, 549–566, doi:10.1175/1520-0469(1988)045<0549:VIACOM>2.0.CO;2.
- , and —, 1990: Ocean wave dynamics and the time scale of ENSO. *J. Phys. Oceanogr.*, **20**, 629–645, doi:10.1175/1520-0485(1990)020<0629:OWDATT>2.0.CO;2.
- Stein, K., N. Schneider, A. Timmermann, and F.-F. Jin, 2010: Seasonal synchronization of ENSO events in a linear stochastic model. *J. Climate*, **23**, 5629–5643, doi:10.1175/2010JCLI3292.1.
- Suarez, M. J., and P. S. Schopf, 1988: A delayed action oscillator for ENSO. *J. Atmos. Sci.*, **45**, 3283–3287, doi:10.1175/1520-0469(1988)045<3283:ADAOFE>2.0.CO;2.
- Thompson, C. J., and D. S. Battisti, 2001: A linear stochastic dynamical model of ENSO. Part II: Analysis. *J. Climate*, **14**, 445–466, doi:10.1175/1520-0442(2001)014<0445:ALSDMO>2.0.CO;2.
- Timmermann, A., 2003: Decadal ENSO amplitude modulations: A nonlinear paradigm. *Global Planet. Change*, **37** (1–2), 135–156, doi:10.1016/S0921-8181(02)00194-7.
- , H. U. Voss, and R. Pasmanter, 2001: Empirical dynamical system modeling of ENSO using nonlinear inverse techniques. *J. Phys. Oceanogr.*, **31**, 1579–1598, doi:10.1175/1520-0485(2001)031<1579:EDSMOE>2.0.CO;2.
- Vecchi, G. A., and D. E. Harrison, 2000: Tropical Pacific sea surface temperature anomalies, El Niño, and equatorial westerly wind events. *J. Climate*, **13**, 1814–1830, doi:10.1175/1520-0442(2000)013<1814:TPSSTA>2.0.CO;2.
- Wu, B., T. Li, and T. Zhou, 2010: Asymmetry of atmospheric circulation anomalies over the western North Pacific between El Niño and La Niña. *J. Climate*, **23**, 4807–4822, doi:10.1175/2010JCLI3222.1.
- Wyrtki, K., 1985: Water displacements in the Pacific and the genesis of El Niño cycles. *J. Geophys. Res.*, **90**, 7129–7132, doi:10.1029/JC090iC04p07129.
- Yu, X., and M. J. McPhaden, 1999: Dynamical analysis of seasonal and interannual variability in the equatorial Pacific. *J. Phys. Oceanogr.*, **29**, 2350–2369, doi:10.1175/1520-0485(1999)029<2350:DAOSAI>2.0.CO;2.
- Zebiak, S. E., 1989: Oceanic heat content variability and El Niño cycles. *J. Phys. Oceanogr.*, **19**, 475–486, doi:10.1175/1520-0485(1989)019<0475:OHCVAE>2.0.CO;2.
- , and M. A. Cane, 1987: A model El Niño–Southern Oscillation. *Mon. Wea. Rev.*, **115**, 2262–2278, doi:10.1175/1520-0493(1987)115<2262:AMENO>2.0.CO;2.